NATIONAL ADVISORY COMMITTEE FOR AERONAUTICS

REPORT No. 747

WIND-TUNNEL TESTS OF FOUR- AND SIX-BLADE SINGLE- AND DUAL-ROTATING TRACTOR PROPELLERS

By DAVID BIERMANN and EDWIN P. HARTMAN

1942

AERONAUTIC SYMBOLS

1. FUNDAMENTAL AND DERIVED UNITS

	Symbol	Metric		English	
		Unit	Abbreviation	Unit	Abbreviation
Length_____	l	meter_____	m	foot (or mile)_____	ft (or mi)
Time_____	t	second_____	s	second (or hour)_____	sec (or hr)
Force_____	F	weight of 1 kilogram_____	kg	weight of 1 pound_____	lb
Power_____	P	horsepower (metric)_____	_____	horsepower_____	hp
Speed_____	V	{kilometers per hour_____ / {meters per second_____	kph / mps	miles per hour_____ / feet per second_____	mph / fps

2. GENERAL SYMBOLS

W Weight$=mg$

g Standard acceleration of gravity$=9.80665$ m/s^2 or 32.1740 ft/sec^2

m Mass$=\dfrac{W}{g}$

I Moment of inertia$=mk^2$. (Indicate axis of radius of gyration k by proper subscript.)

μ Coefficient of viscosity

ν Kinematic viscosity

ρ Density (mass per unit volume)

Standard density of dry air, 0.12497 kg-m^{-4}-s^2 at 15° C and 760 mm; or 0.002378 lb-ft^{-4} sec^2

Specific weight of "standard" air, 1.2255 kg/m^3 or 0.07651 lb/cu ft

3. AERODYNAMIC SYMBOLS

S Area

S_w Area of wing

G Gap

b Span

c Chord

A Aspect ratio, $\dfrac{b^2}{S}$

V True air speed

q Dynamic pressure, $\dfrac{1}{2}\rho V^2$

L Lift, absolute coefficient $C_L=\dfrac{L}{qS}$

D Drag, absolute coefficient $C_D=\dfrac{D}{qS}$

D_0 Profile drag, absolute coefficient $C_{D_0}=\dfrac{D_0}{qS}$

D_i Induced drag, absolute coefficient $C_{D_i}=\dfrac{D_i}{qS}$

D_p Parasite drag, absolute coefficient $C_{D_p}=\dfrac{D_p}{qS}$

C Cross-wind force, absolute coefficient $C_c=\dfrac{C}{qS}$

i_w Angle of setting of wings (relative to thrust line)

i_t Angle of stabilizer setting (relative to thrust line)

Q Resultant moment

Ω Resultant angular velocity

R Reynolds number, $\rho\dfrac{Vl}{\mu}$ where l is a linear dimension (e.g., for an airfoil of 1.0 ft chord, 100 mph, standard pressure at 15° C, the corresponding Reynolds number is 935,400; or for an airfoil of 1.0 m chord, 100 mps, the corresponding Reynolds number is 6,865,000)

α Angle of attack

ϵ Angle of downwash

α_0 Angle of attack, infinite aspect ratio

α_i Angle of attack, induced

α_a Angle of attack, absolute (measured from zero-lift position)

γ Flight-path angle

2626°

REPORT No. 747

WIND-TUNNEL TESTS OF FOUR- AND SIX-BLADE SINGLE- AND DUAL-ROTATING TRACTOR PROPELLERS

By DAVID BIERMANN and EDWIN P. HARTMAN

Langley Memorial Aeronautical Laboratory

Langley Field, Va.

NATIONAL ADVISORY COMMITTEE FOR AERONAUTICS

HEADQUARTERS, 1500 NEW HAMPSHIRE AVENUE NW., WASHINGTON, D. C.

Created by act of Congress approved March 3, 1915, for the supervision and direction of the scientific study of the problems of flight (U. S. Code, title 50, sec. 151). Its membership was increased to 15 by act approved March 2, 1929. The members are appointed by the President, and serve as such without compensation.

TECHNICAL COMMITTEES

AERODYNAMICS   **AIRCRAFT MATERIALS**   **INVENTIONS & DESIGNS**
POWER PLANTS FOR AIRCRAFT   **AIRCRAFT STRUCTURES**   **OPERATING PROBLEMS**

Coordination of Research Needs of Military and Civil Aviation

Preparation of Research Programs

Allocation of Problems

Prevention of Duplication

Consideration of Inventions

LANGLEY MEMORIAL AERONAUTICAL LABORATORY   **AMES AERONAUTICAL LABORATORY**
LANGLEY FIELD, VA.   MOFFETT FIELD, CALIF.

AIRCRAFT ENGINE RESEARCH LABORATORY
CLEVELAND AIRPORT, CLEVELAND, OHIO

Conduct, under unified control, for all agencies, of scientific research on the fundamental problems of flight.

OFFICE OF AERONAUTICAL INTELLIGENCE
WASHINGTON, D. C.

Collection, classification, compilation, and dissemination of
scientific and technical information on aeronautics

REPORT No. 747

WIND-TUNNEL TESTS OF FOUR- AND SIX-BLADE SINGLE- AND DUAL-ROTATING TRACTOR PROPELLERS

By David Biermann and Edwin P. Hartman

SUMMARY

Tests of 10-foot diameter, four- and six-blade single-rotating and dual-rotating propellers were conducted in the NACA propeller-research tunnel. The propellers were mounted at the front end of a streamline body incorporating spinners to house the hub portions. The effect of a symmetrical wing mounted in the slipstream was investigated. The blade angles investigated ranged from 20° to 65°; the 65° setting corresponds to airplane speeds greater than 500 miles per hour.

The results indicate that dual-rotating propellers were from 0 to 6 percent more efficient than single-rotating ones; but, when the propellers operated in the presence of a wing, the gain was reduced about one-half. Other advantages of dual-rotating propellers were found to include greater power absorption and greater efficiency at the low V/nD operating range of high-pitch propellers.

INTRODUCTION

Theoretical treatments of propeller losses, such as those given in references 1 and 2, have indicated rotational losses in the slipstream amounting to several percent for highly loaded propellers operating at high values of V/nD. Military aircraft have now reached the stage of speed and power wherein it appears that dual-rotating propellers might be justified on the grounds of improved efficiency alone although the elimination of the engine torque reaction might be a more important consideration. In view of these advantages of dual-rotating propellers over single-rotating ones, the need for full-scale propeller tests is obvious, inasmuch as very little information on the subject is available.

A test program was instituted for the propeller-research tunnel to cover the following conditions: Tests of two-, three-, four-, six-, and eight-blade single-rotating propellers operating both as tractors and pushers; tests of four-, six-, and eight-blade dual-rotating propellers operating both as tractors and pushers; tests to determine the effect of a wing in reducing the slipstream rotational losses.

The present report covers the results of the tractor tests made with four- and six-blade single-rotating and four- and six-blade dual-rotating propellers operating with and without a wing in the slipstream.

APPARATUS AND METHODS

The tests were made in the NACA propeller-research tunnel.

Propellers.—The propellers, which incorporate the Clark Y section, were approximately 10 feet in diameter. They varied slightly in diameter, depending on the hub used. The drawing numbers are Hamilton Standard 3155–6 for the right-hand blades and Hamilton Standard 3156–6 for the left-hand blades. Blade-form curves are given in figure 1.

Driving mechanism.—The propellers were driven by two 25-horsepower electric motors arranged in tandem. (See fig. 2.) The front motor was directly connected to the front propeller and the rear motor drove the rear propeller through chains and a countershaft. The propeller shafts were locked together for
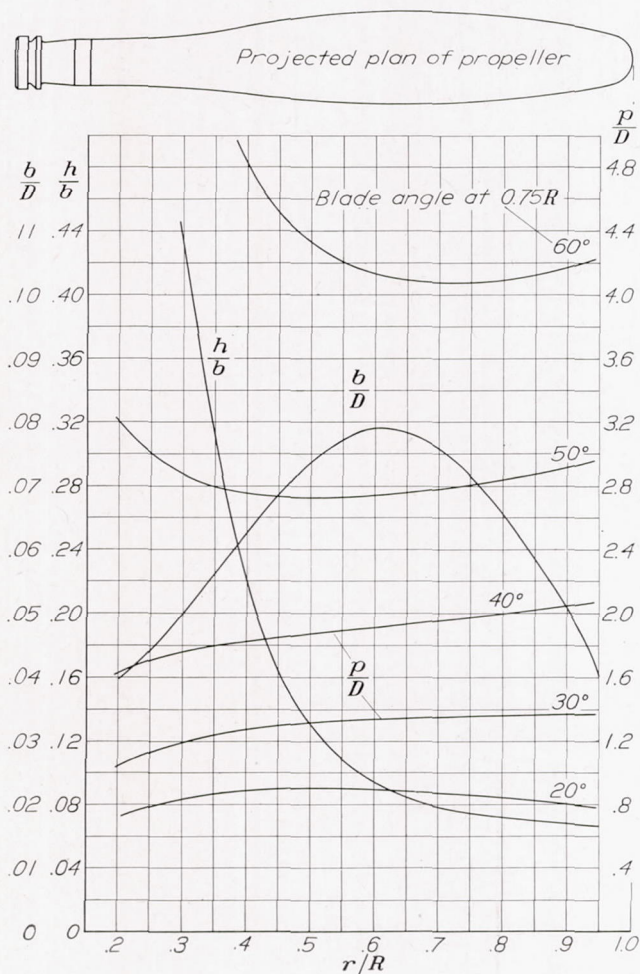
FIGURE 1.—Plan-form and blade-form curves for propellers 3155–6 and 3156–6. D, diameter; R, radius to the tip; r, station radius; b, section chord; h, section thickness; p, geometric pitch.

1

single-rotation operating conditions. The motors were mounted on bearings concentric with the shaft axis. Each motor frame was restrained from rotating by helical springs connecting with the supporting frame,
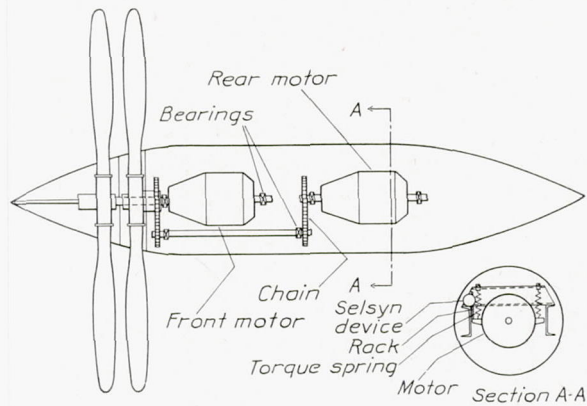
FIGURE 2.—Propeller-drive mechanism.

which provided means of measuring the torque. Selsyn devices were used to transmit the motion of the motor frames to the test chamber in order that torque measurements could be made.
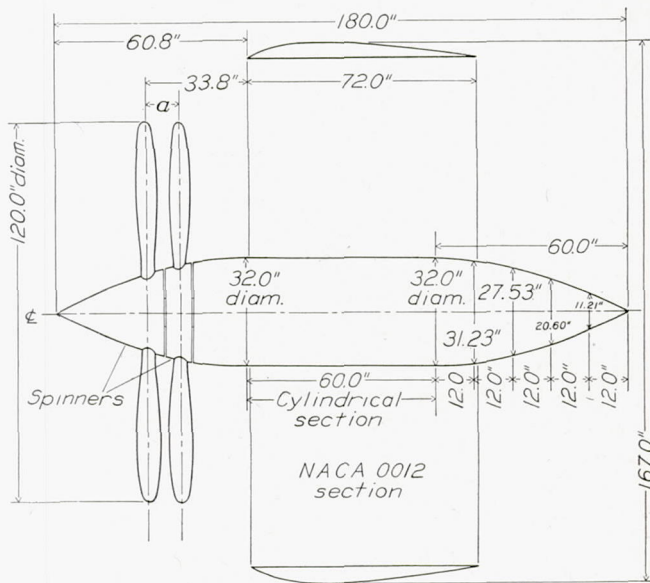
FIGURE 3.—Plan view showing dimensional details of wing and nacelle. Dimension *a* for four-blade propeller=9.7 inches and for six-blade propeller=10.0 inches. Front and rear nacelle lines are identical.

Body.—An outline of the streamline body housing the motors is shown in figure 3. A photograph of the setup is given in figure 4. Tests were made with and without the symmetrical wing in place. The wing was located in the midwing position and set at an angle of attack of 0°. Both ends of the body were made identical in order that comparative tractor and pusher tests could be made without altering the body shape. Spinners were used for all tests. Both wing and body were constructed of wooden forming members covered with sheet-aluminum skin.

Measuring equipment.—The net thrust or drag of the propeller-body combination was measured on a thrust balance located on the floor of the test chamber. The torque of each motor was measured with the spring-dynamometer Selsyn repeating system. The dynamometer was calibrated before and after the series of tests was made. Friction-determination tests were made frequently during the program. The propeller speed was measured with an accurate electric tachometer checked frequently during the investigation. Each propeller of the dual combinations was run at the same
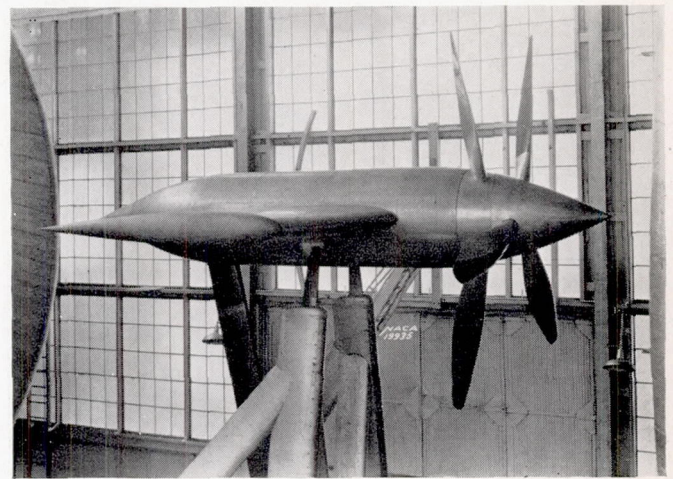
FIGURE 4.—Test setup. The photograph shows a six-blade single-rotating propeller with wing in place.

speed. A synchroscope was used to indicate synchronism. Control of the relative speeds of the two motors was obtained with a frequency converter placed in the line feeding one of the induction drive motors.

Test conditions.—The tunnel speed ranged from zero to about 110 miles per hour. The maximum propeller speed was about 550 rpm, which corresponds to a rotational tip speed of 287 feet per second.

The dual-rotation tests were made with the rear propeller blades adjusted to provide approximately the same torque at peak efficiency as for the front propeller. A plot of the difference between the front and the rear propeller-blade settings is given in figure 5. A typical plot of the results is given in figure 6. The amount that the test points scatter gives an indication of the accuracy of the results.

The four- and the six-blade single-rotating propellers were made up with two two-way and three-way hubs, respectively, mounted in tandem. Because of the position of the shaft splines when the shafts were keyed together, equal spacing between front and rear blades was impossible and therefore the front blade led the rear by 85.4° and 75.0° for four-blade and six-blade propellers, respectively. This arrangement resulted in identical blade shank and spinner conditions for both the single- and dual-rotation tests.
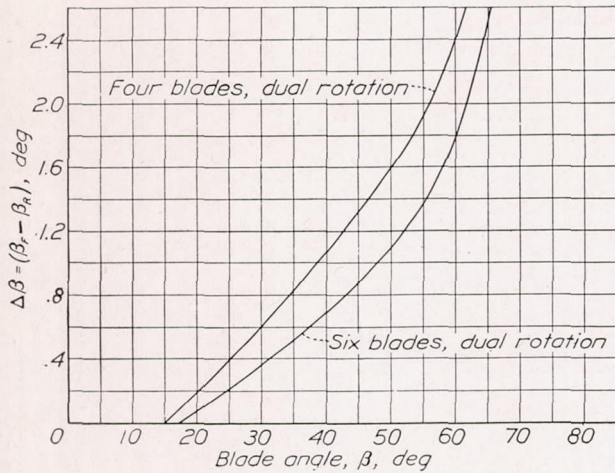
FIGURE 5.—Difference between front and rear blade setting for dual-rotating propellers.
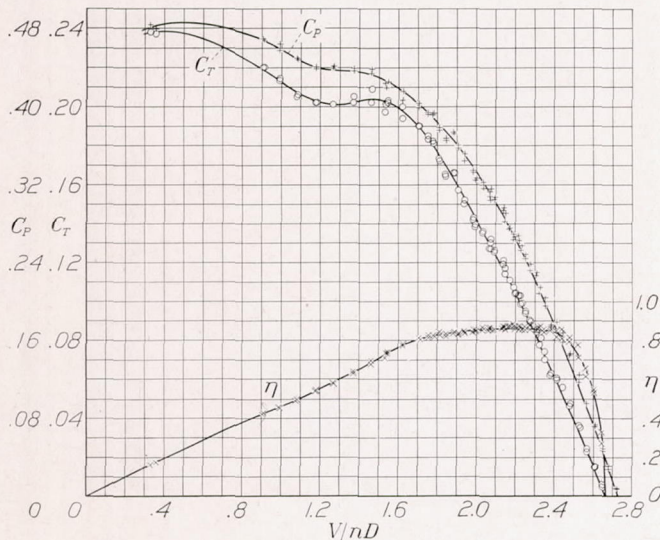
FIGURE 6.—Typical test results. Four-blade single rotation with wing. Propeller set 45° at 0.75R.

RESULTS AND DISCUSSION

The measured values have been reduced to the usual coefficients of thrust, power, and propulsive efficiency.

$$C_T = \frac{\text{effective thrust}}{\rho n^2 D^4}$$

$$C_P = \frac{P}{\rho n^3 D^5}$$

$$\eta = \frac{C_T}{C_P} \frac{V}{nD}$$

$$C_s = \sqrt[5]{\frac{\rho V^5}{P n^2}} \text{ or } \frac{V/nD}{\sqrt[5]{C_P}}$$

where the effective thrust is the measured thrust of the propeller-body combination plus the drag of the body measured separately, and

D propeller diameter, feet

n propeller rotational speed, revolutions per second

ρ mass density of air, slugs per cubic foot

V airspeed, feet per second

P engine power, foot-pounds per second

Other symbols used in the charts are:

β blade angle at 0.75R, degrees

R propeller radius, feet

β_F front blade angle at 0.75R, degrees

β_R rear blade angle at 0.75R, degrees

C_{P_F} power coefficient for front propeller

C_{P_R} power coefficient for rear propeller

C_{T_D} thrust coefficient for dual rotation

C_{T_S} thrust coefficient for single rotation

These coefficients were plotted against V/nD. The results are given in the following figures:

Figure	Number of blades	Rotation	Wing
7 to 9	4	Single	Without.
10 to 13	4	Dual	Without.
14 to 16	6	Single	Without.
17 to 20	6	Dual	Without.
21 to 23	4	Single	With.
24 to 27	4	Dual	With.
28 to 30	6	Single	With.
31 to 34	6	Dual	With.
35 to 36	Effect of small variations in blade angles for dual propeller.		
37	Envelope-efficiency comparisons.		
38 to 39	Comparisons of power absorbed.		
40	Comparisons of thrust available at constant power.		
41 to 44	Design charts for propellers 3155–6 and 3156–6.		

In addition to the comparisons listed, several direct comparisons are made between the six-blade single- and dual-propeller characteristics in figures 17 to 20 and figures 31 to 34. In each case where the single-rotation curves have been superimposed on the dual-rotation curves, the single-rotation curves have been interpolated to coincide with the dual-rotation curves for the condition of zero C_T and η.

The dual-rotation tests were conducted with the rear propeller set at a slightly lower angle than the front one in order to absorb approximately the same power at the peak-efficiency condition. (See fig. 5 for blade settings.) The necessity for this difference in blade angle can be explained by the fact that the front propeller introduces a rotational component to the slipstream that increases the effective rotational velocity as well as the angle of attack of the rear propeller. It is then necessary to reduce the blade angle of the rear propeller to offset these factors.

The front propeller also adds energy to the stream in the form of an increment of pressure across the propeller disk. The pressure energy is gradually converted into velocity energy as the flow progresses. For closely spaced dual-rotating propellers the velocity through the rear propeller disk is very little different from that through the front propeller disk, hence the blade-angle increment of the rear propeller necessary to offset this increased velocity is probably very little. If the propeller spacing were large, the velocity factor would be quite perceptible and, in the case of low-pitch propellers, might even overbalance the rotational factor.
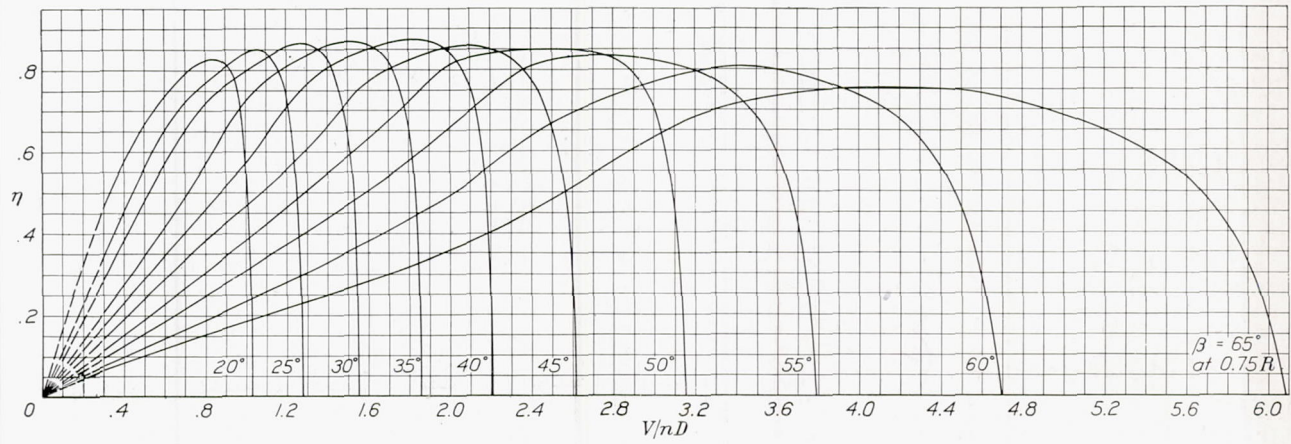
FIGURE 7.—Efficiency curves for four-blade single-rotating propeller without wing.
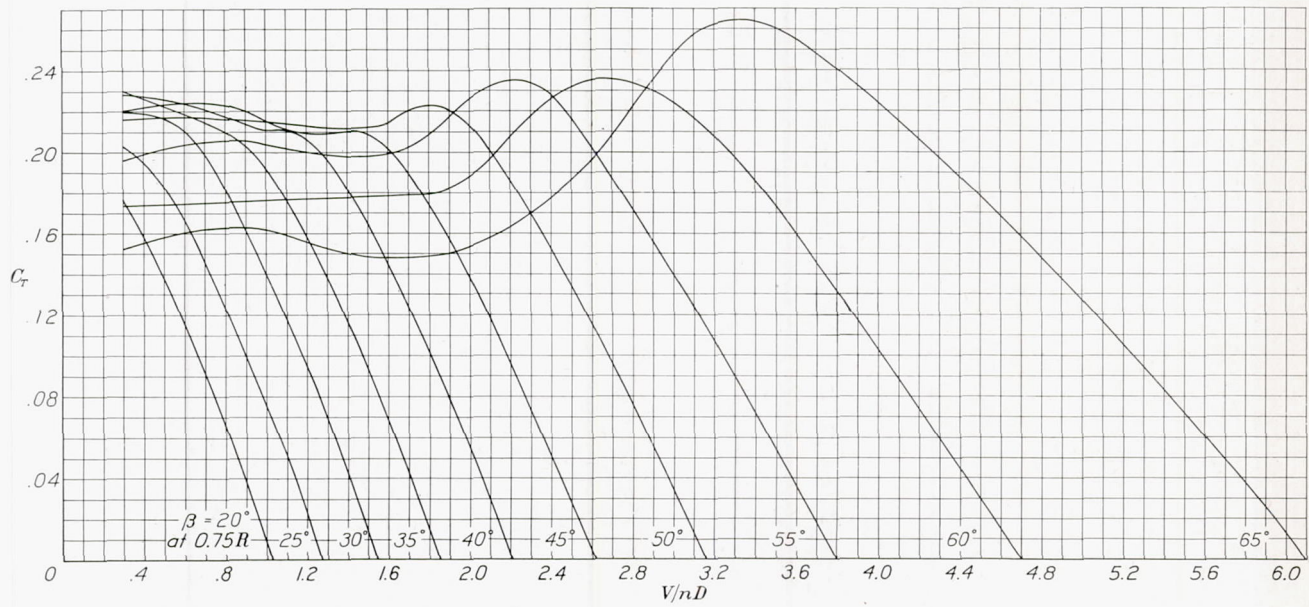
FIGURE 8.—Thrust-coefficient curves for four-blade single-rotating propeller without wing.
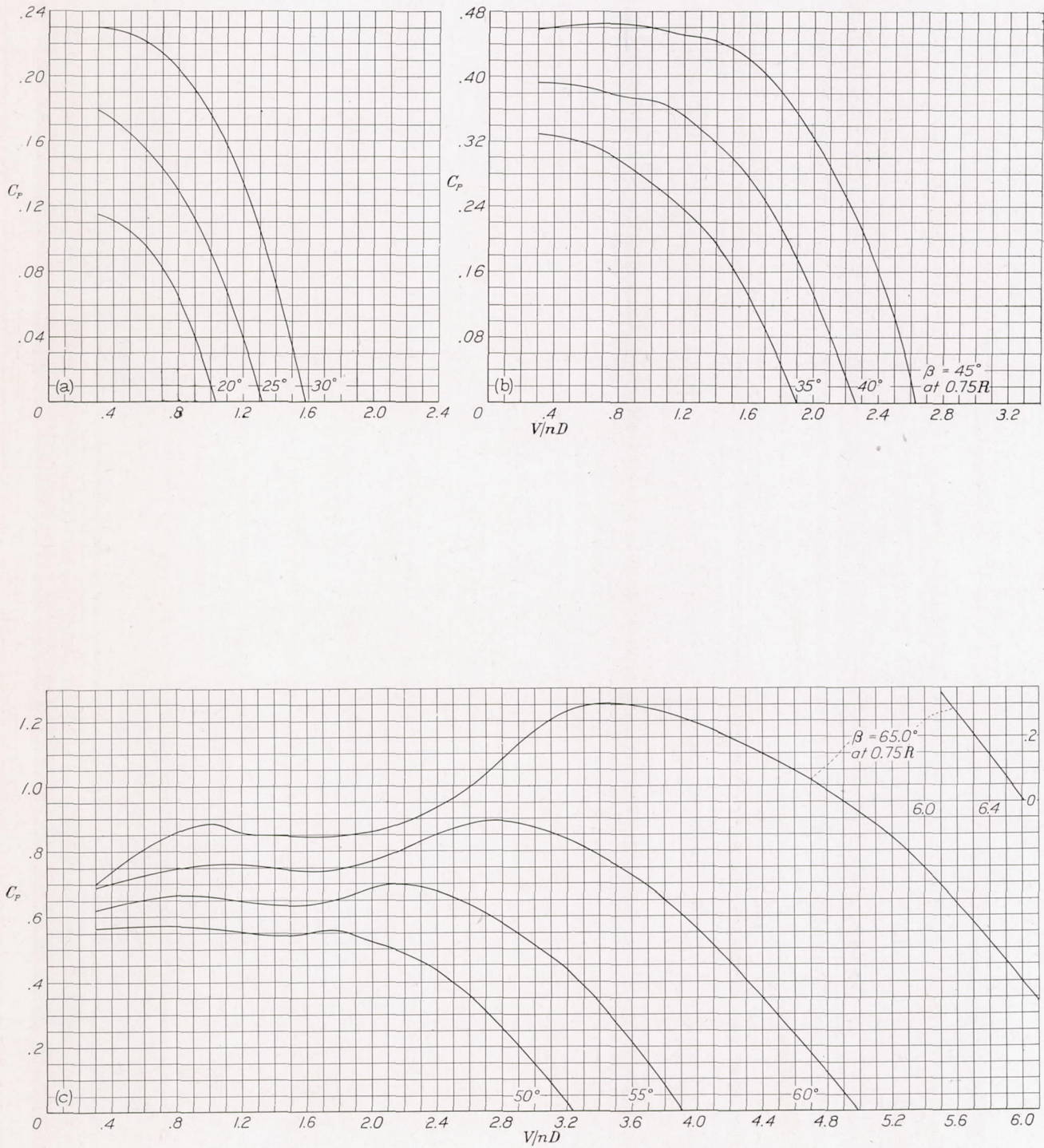
FIGURE 9.—Power-coefficient curves for four-blade single-rotating propeller without wing.
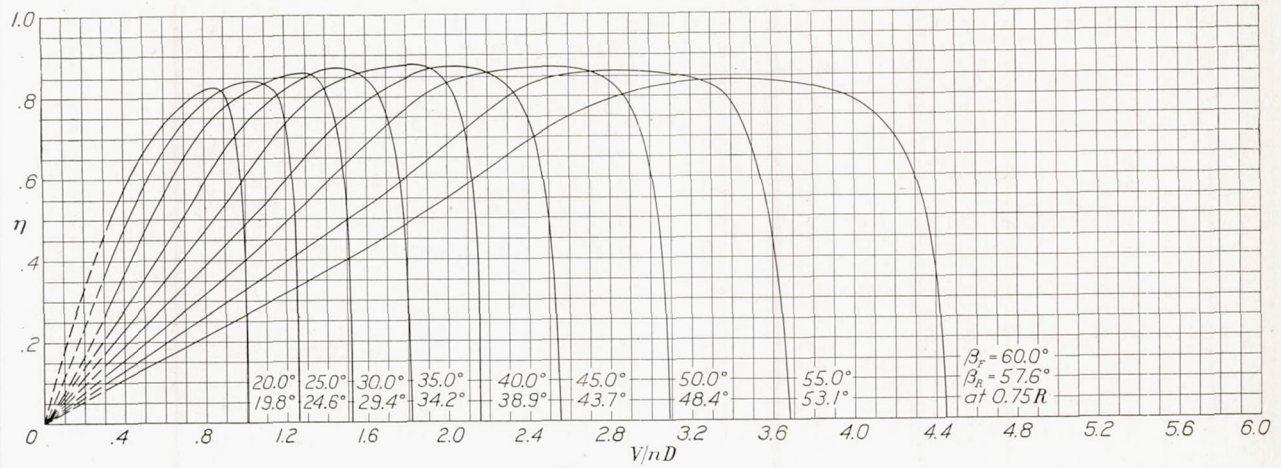
FIGURE 10.—Efficiency curves for four-blade dual-rotating propellers without wing.
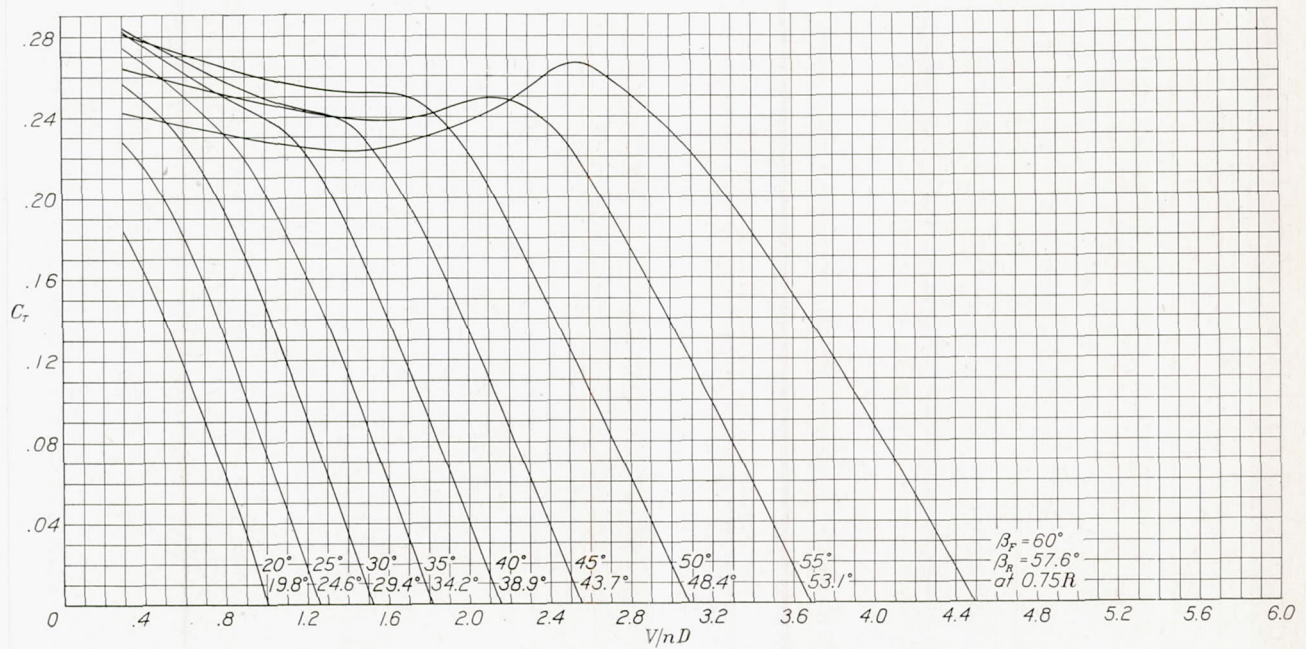
FIGURE 11.—Thrust-coefficient curves for four-blade dual-rotating propellers without wing.
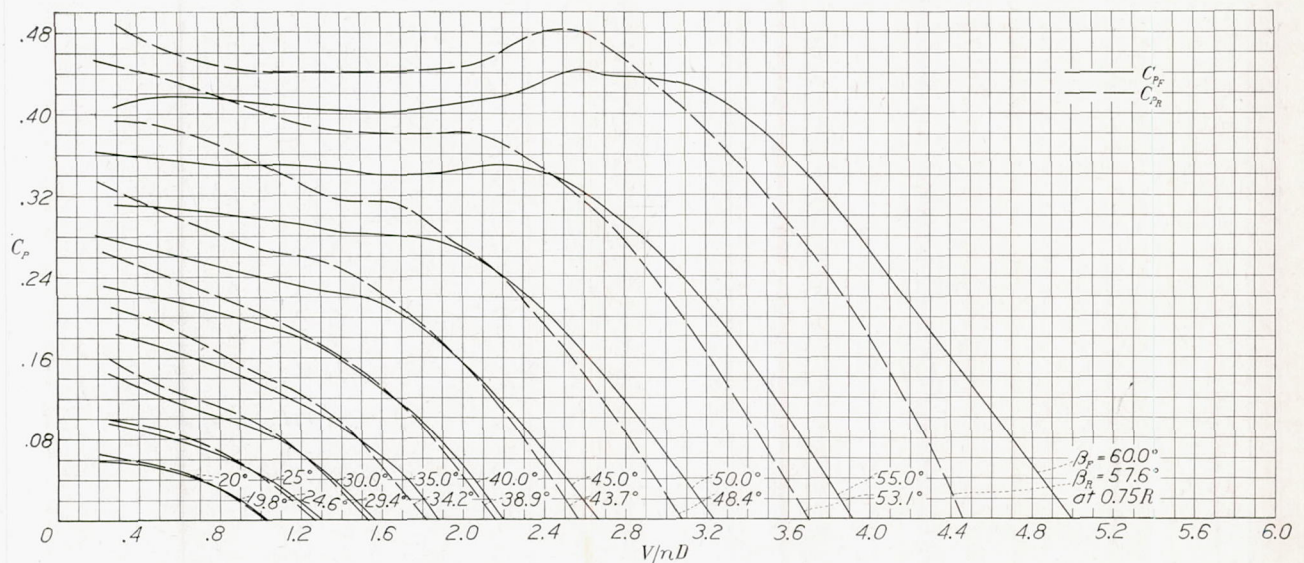
FIGURE 12.—Individual power-coefficient curves for four-blade dual-rotating propellers without wing.
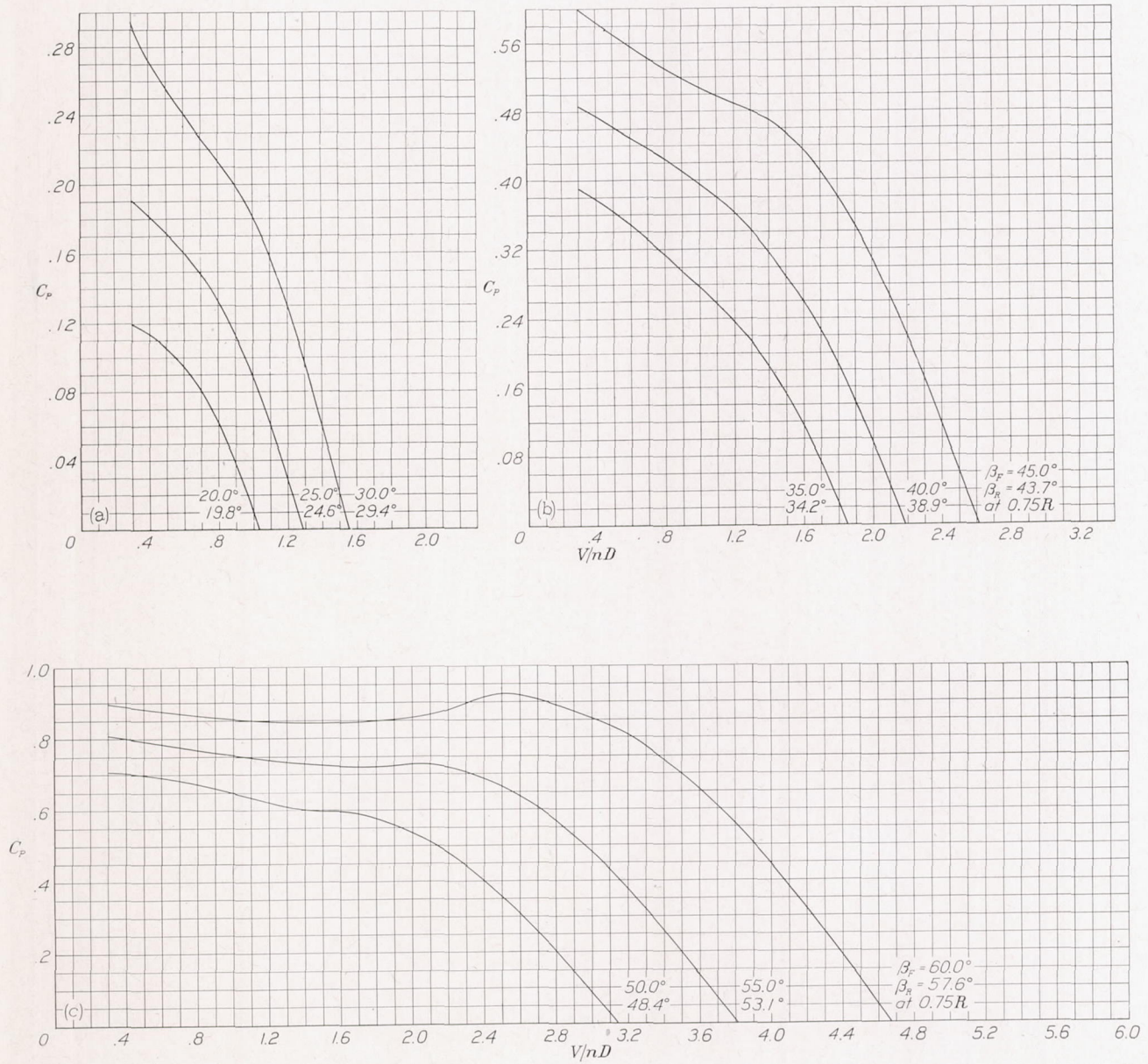
FIGURE 13.—Power-coefficient curves for four-blade dual-rotating propellers without wing.
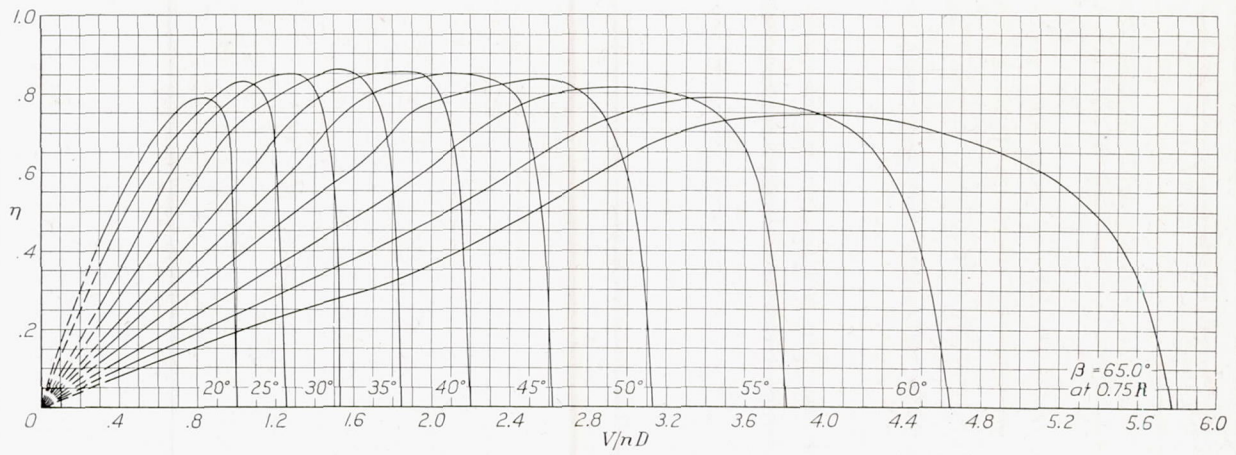
FIGURE 14.—Efficiency curves for six-blade single-rotating propeller without wing.
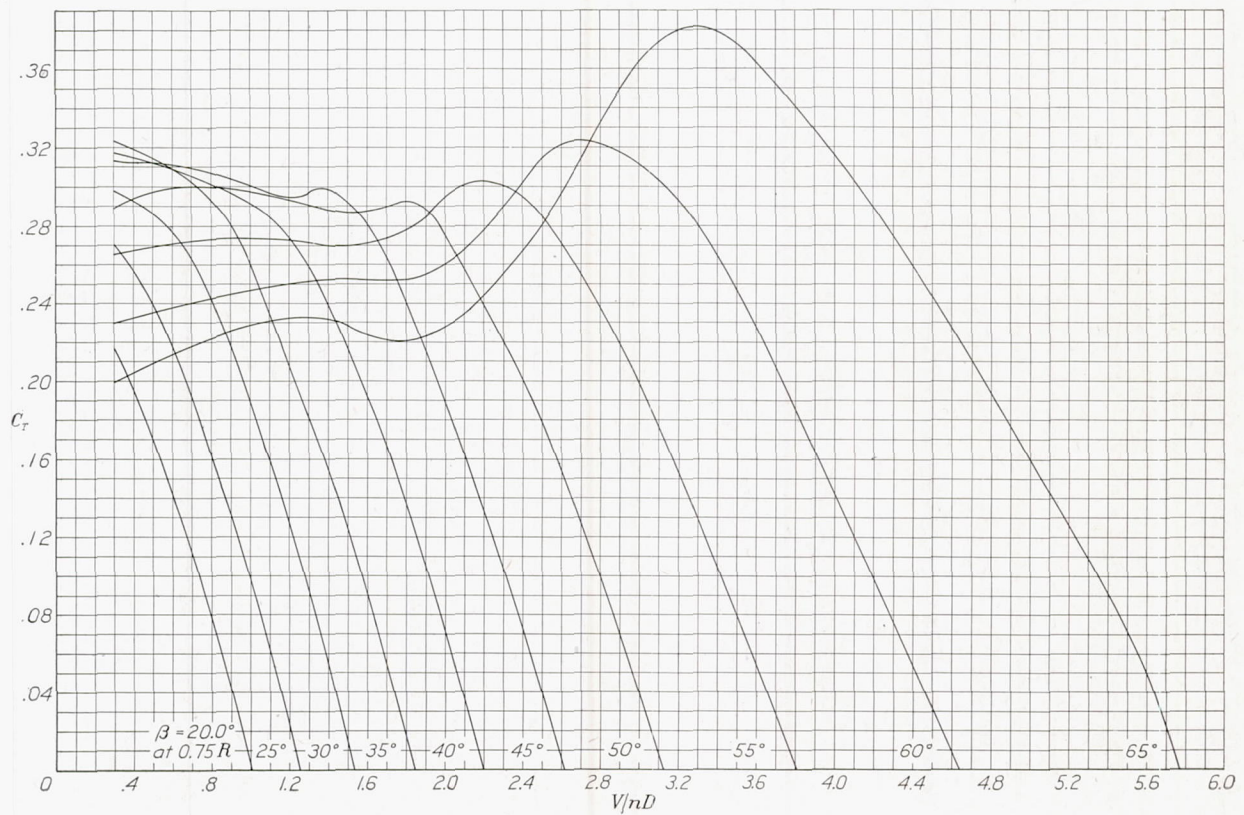
FIGURE 15.—Thrust-coefficient curves for six-blade single-rotating propeller without wing.
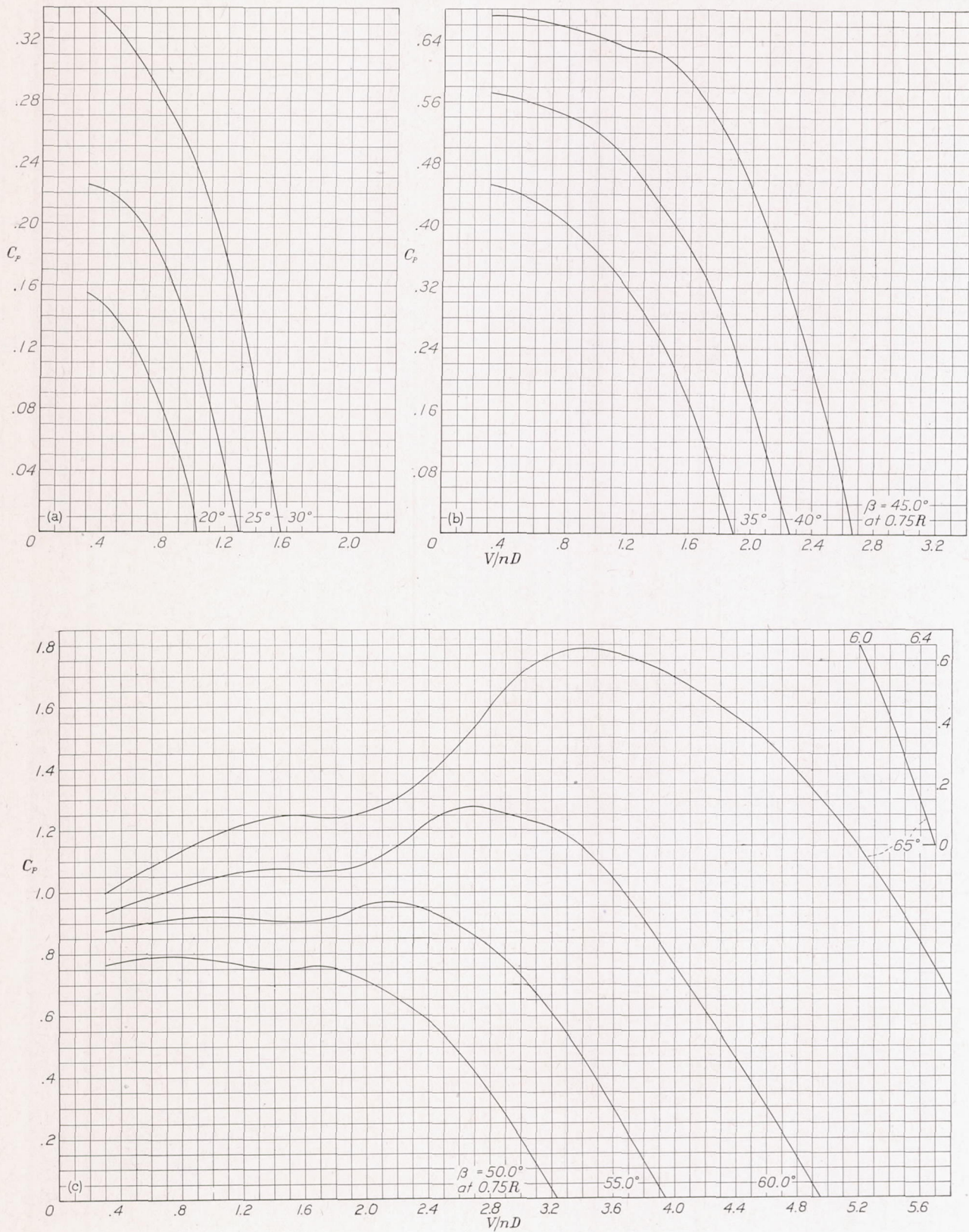
FIGURE 16.—Power-coefficient curves for six-blade single-rotating propeller without wing.
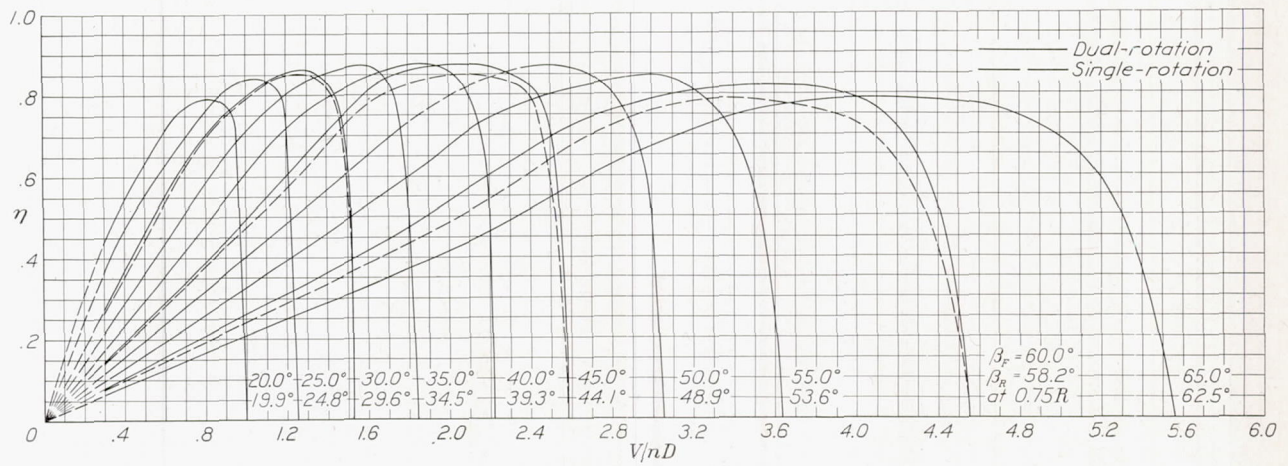
FIGURE 17.—Efficiency curves for six-blade dual-rotating propellers without wing, showing superimposed curves for the corresponding single-rotation condition at 30°, 45° and 60° blade angles.
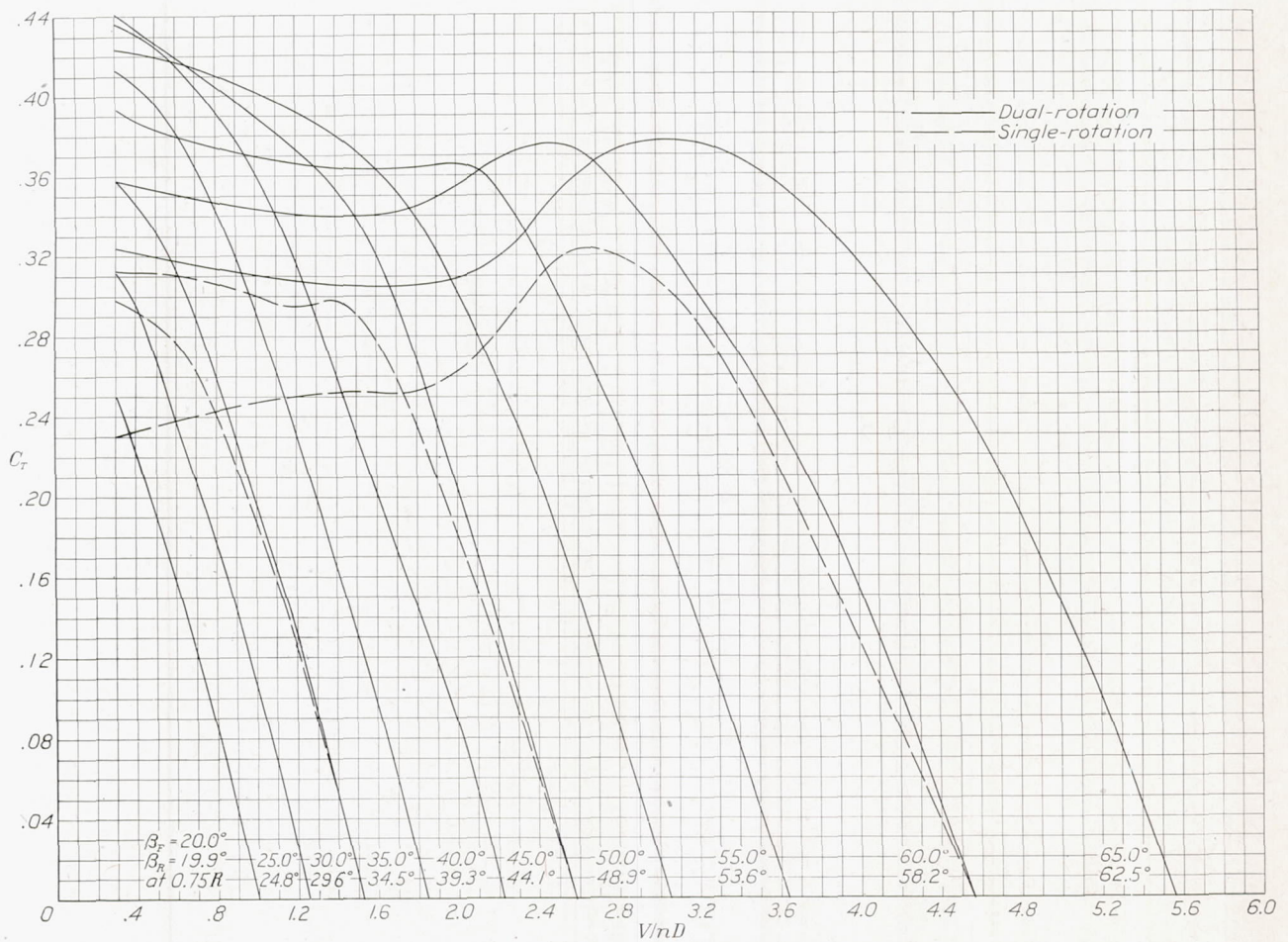
FIGURE 18.—Thrust-coefficient curves for six-blade dual-rotating propellers without wing, showing superimposed curves for the corresponding single-rotation condition at 30°, 45°, and 60° blade angles.
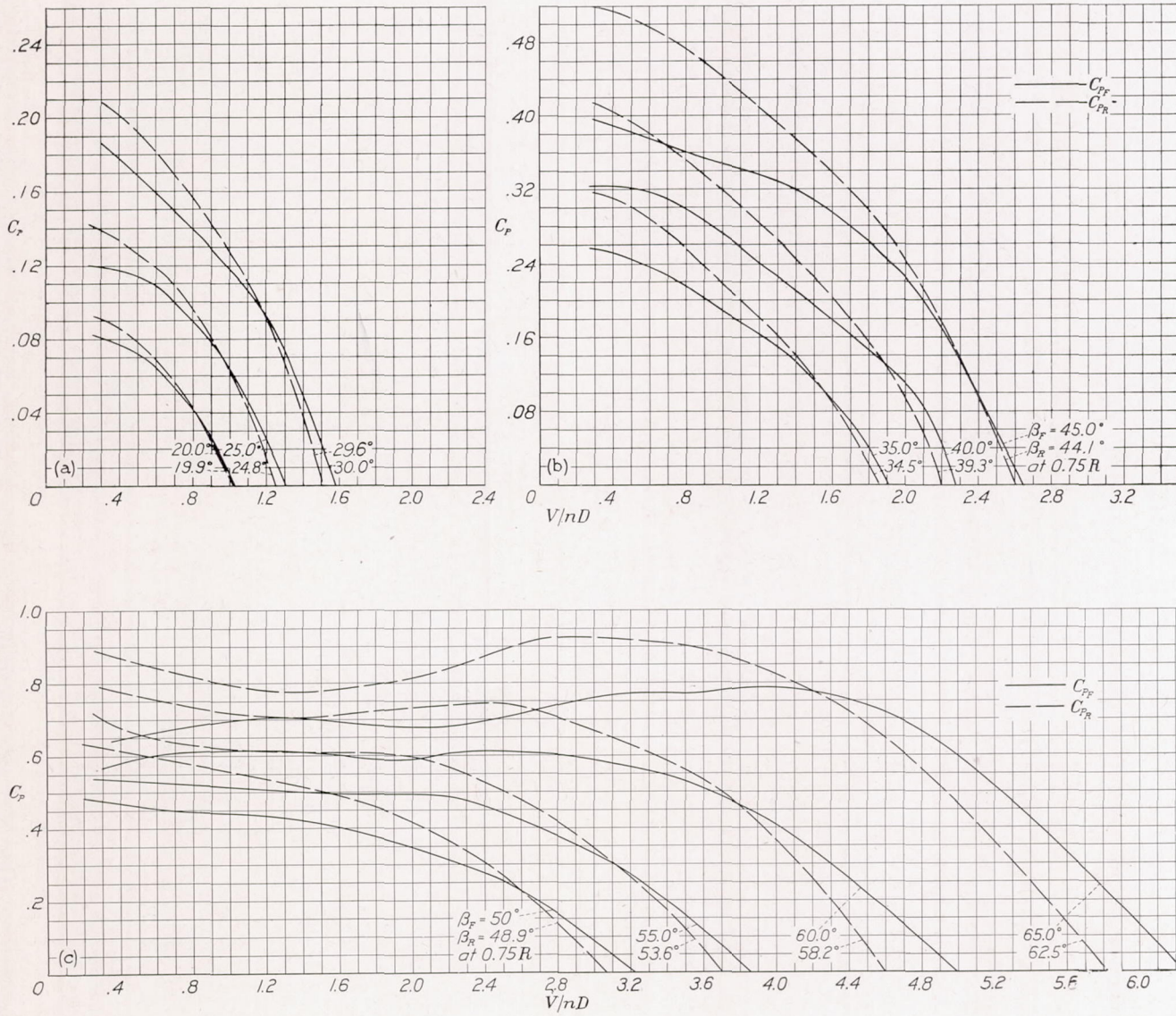
FIGURE 19.—Individual power-coefficient curves for six-blade dual-rotating propellers without wing.

(a) 30° blade angle.

(b) 45° blade angle.

(c) 60° blade angle.
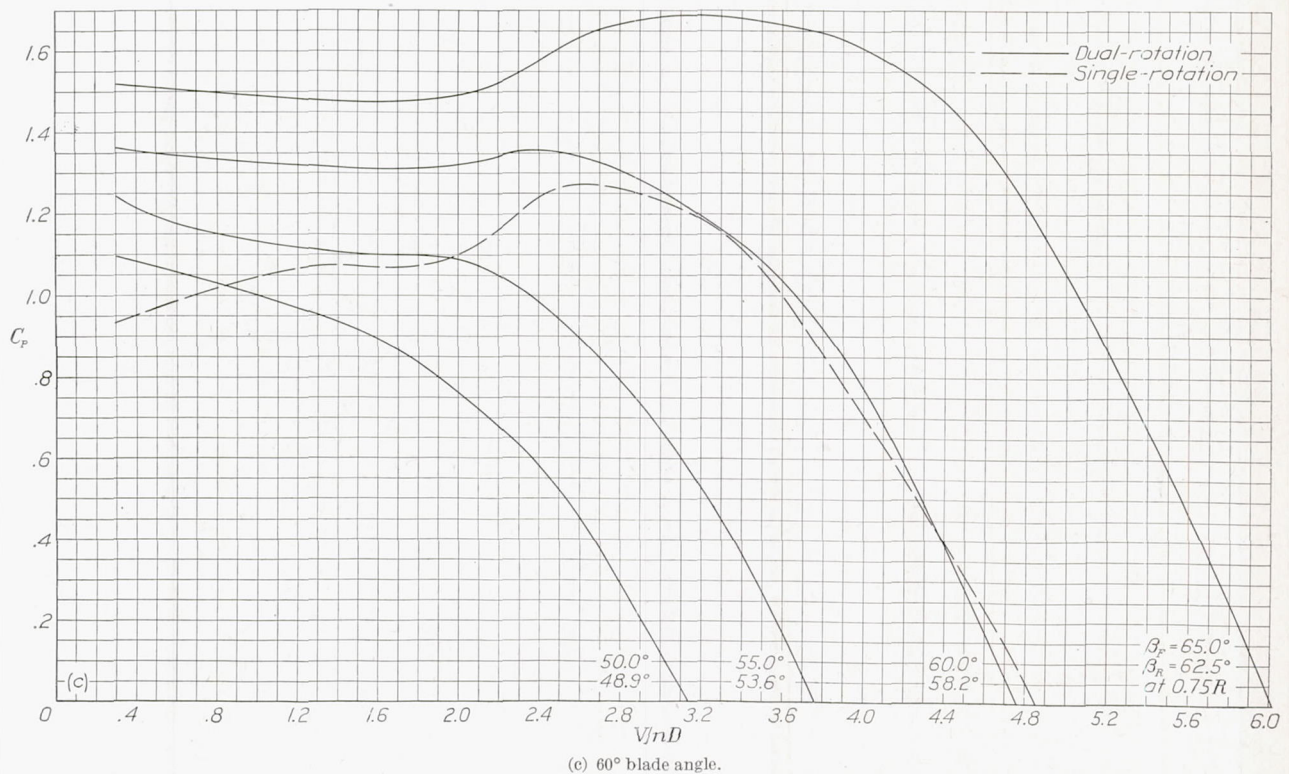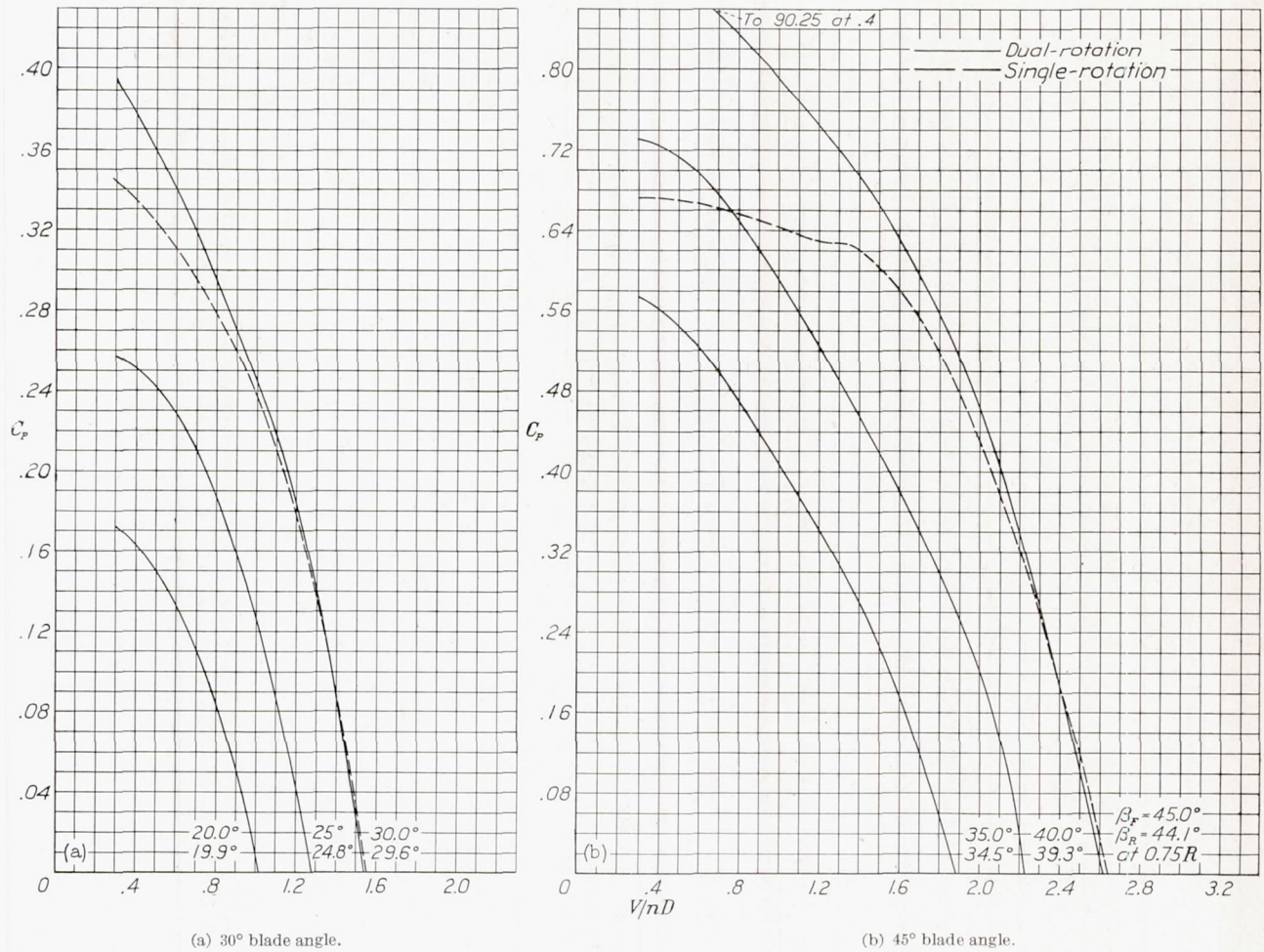
FIGURE 20.—Power-coefficient curves for six-blade dual-rotating propellers without wing, showing superimposed curve for the corresponding single-rotation condition.
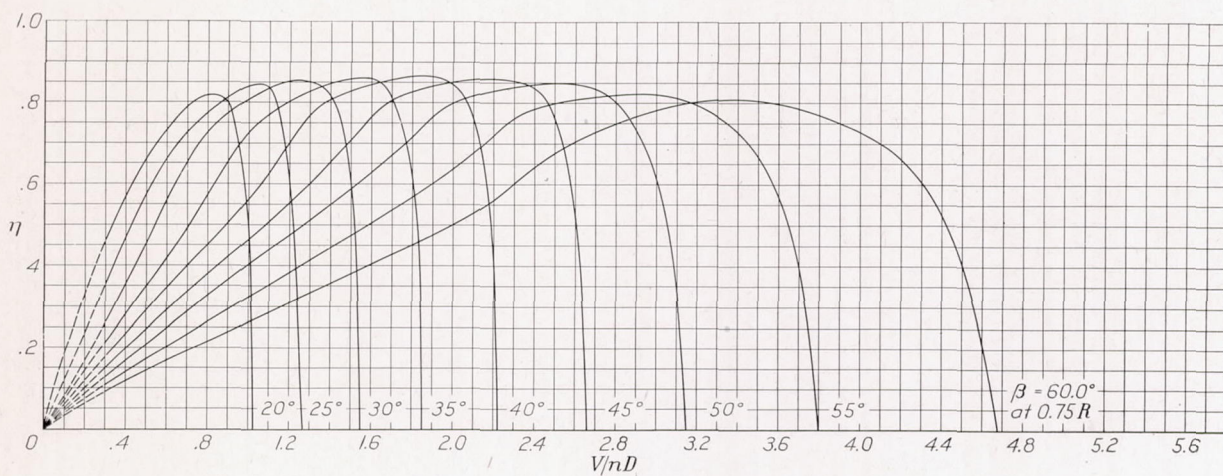
FIGURE 21.—Efficiency curves for four-blade single-rotating propeller with wing.
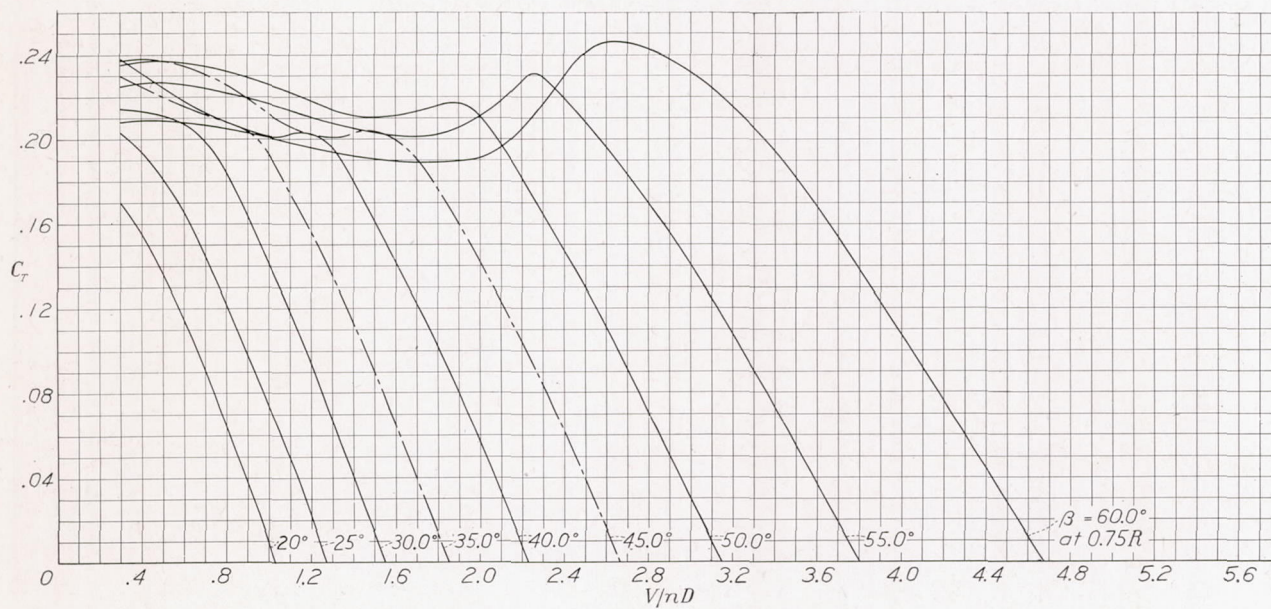
FIGURE 22.—Thrust-coefficient curves for four-blade single-rotating propeller with wing.
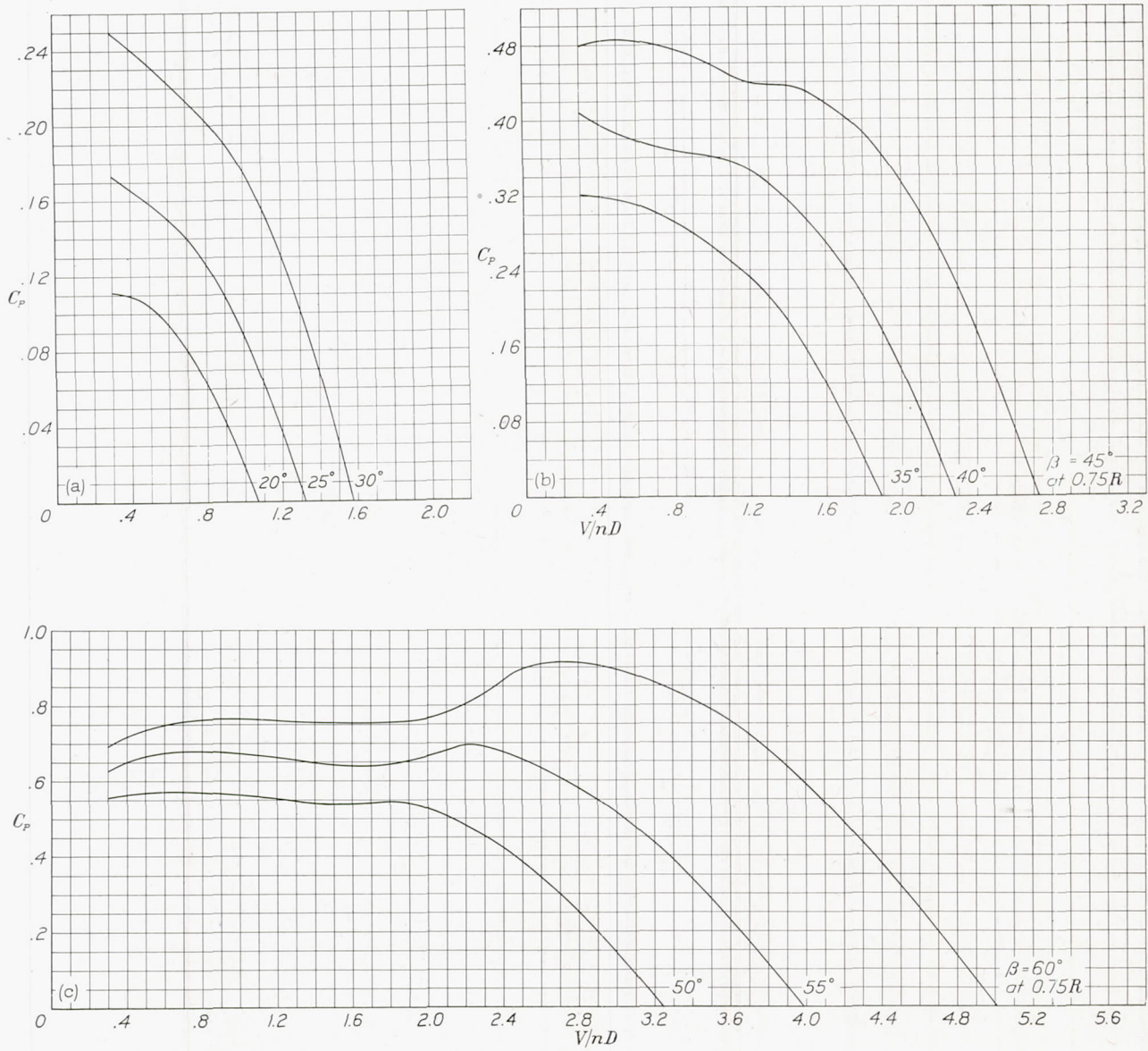
FIGURE 23.—Power-coefficient curves for four-blade single-rotating propeller with wing.
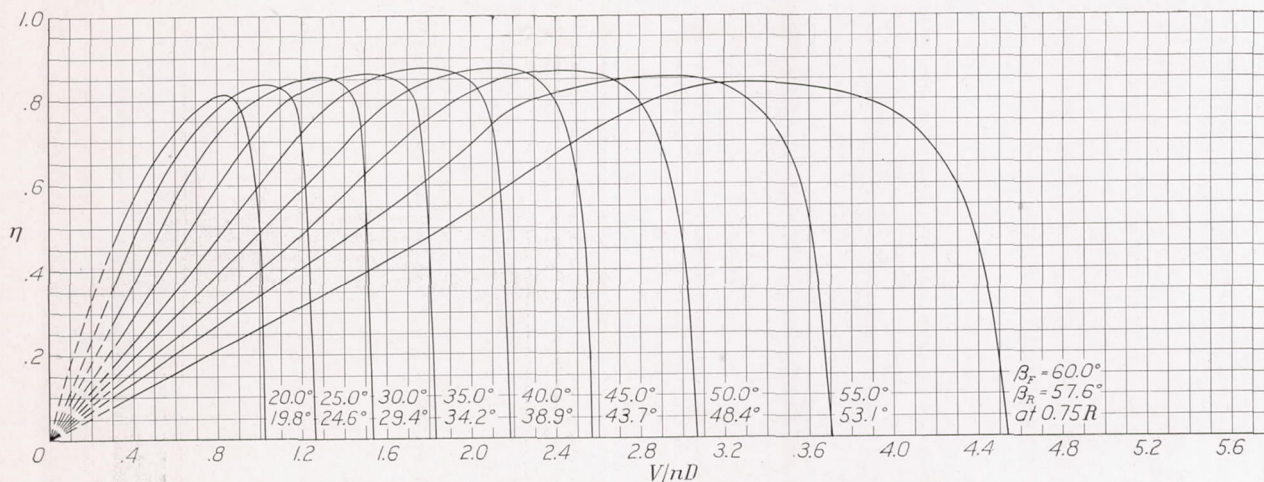
FIGURE 24.—Efficiency curves for four-blade dual-rotating propellers with wing.
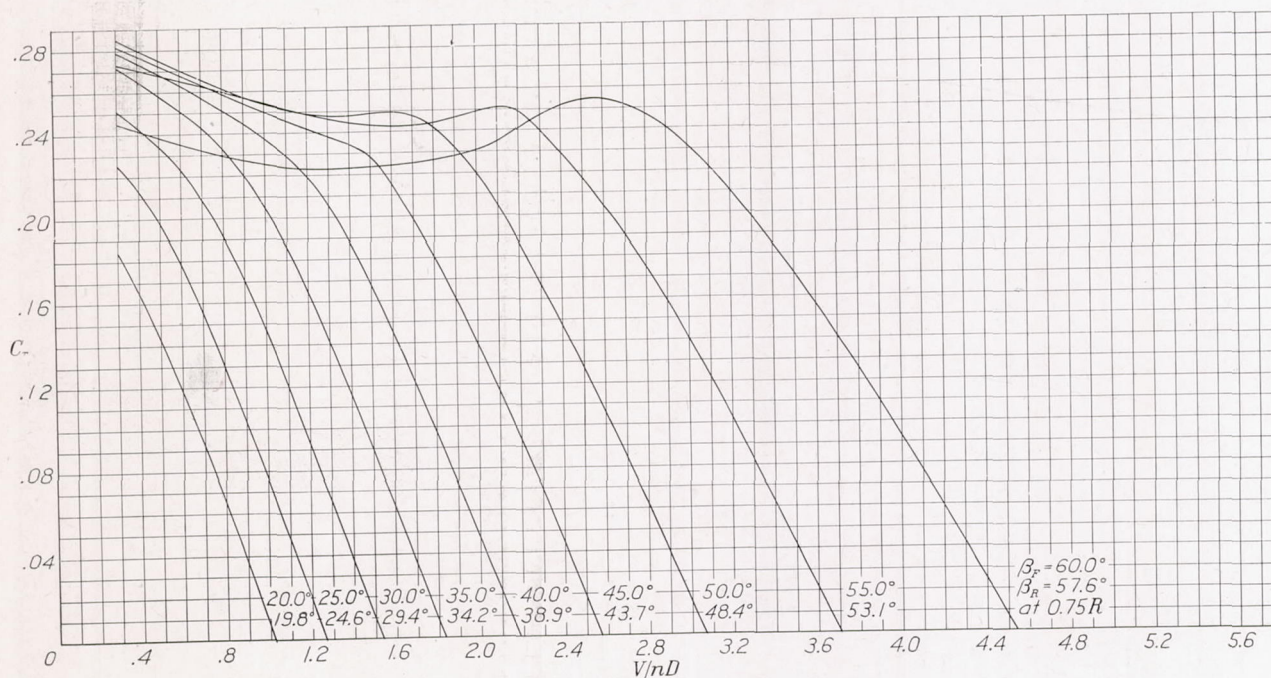
FIGURE 25.—Thrust-coefficient curves for four-blade dual-rotating propellers with wing.
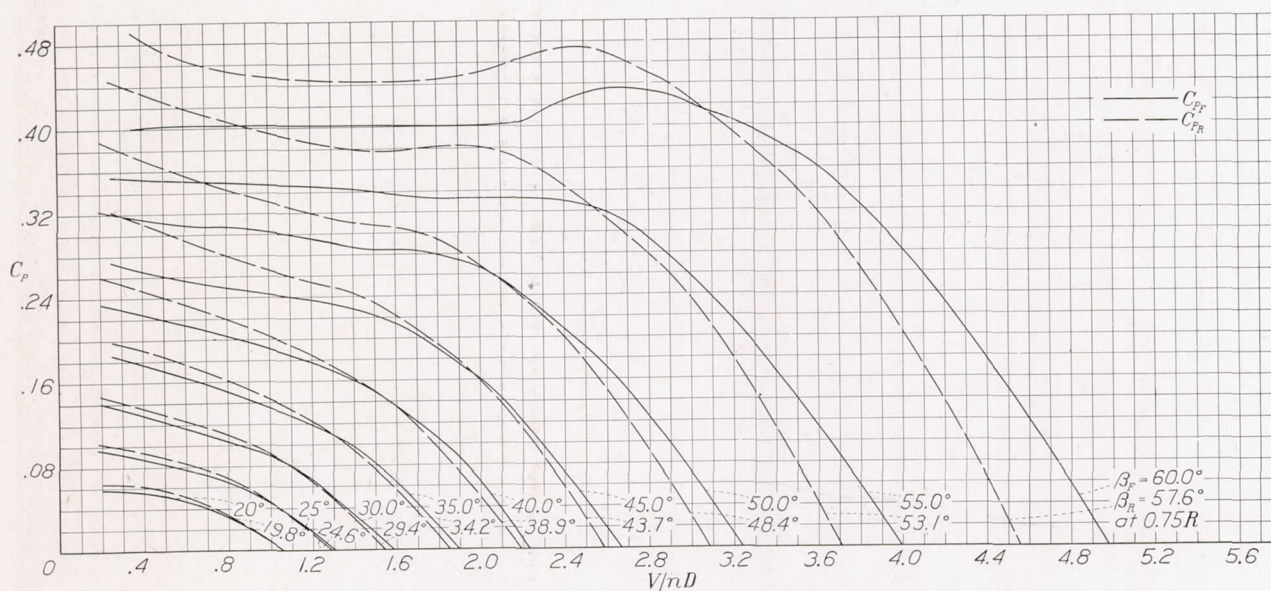
FIGURE 26.—Individual power-coefficient curves for four-blade dual-rotating propellers with wing.
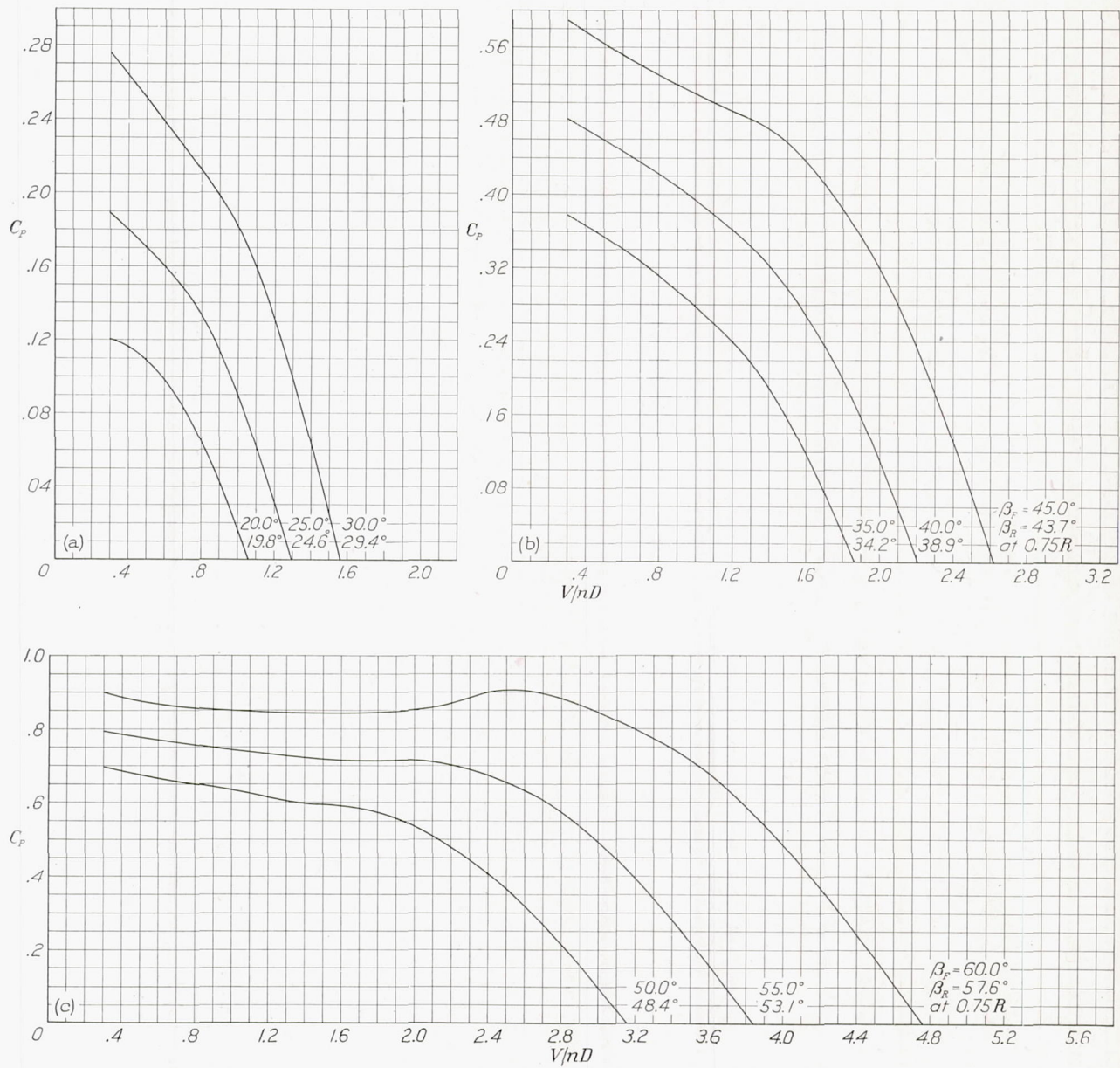
FIGURE 27.—Power-coefficient curves for four-blade dual-rotating propellers with wing.
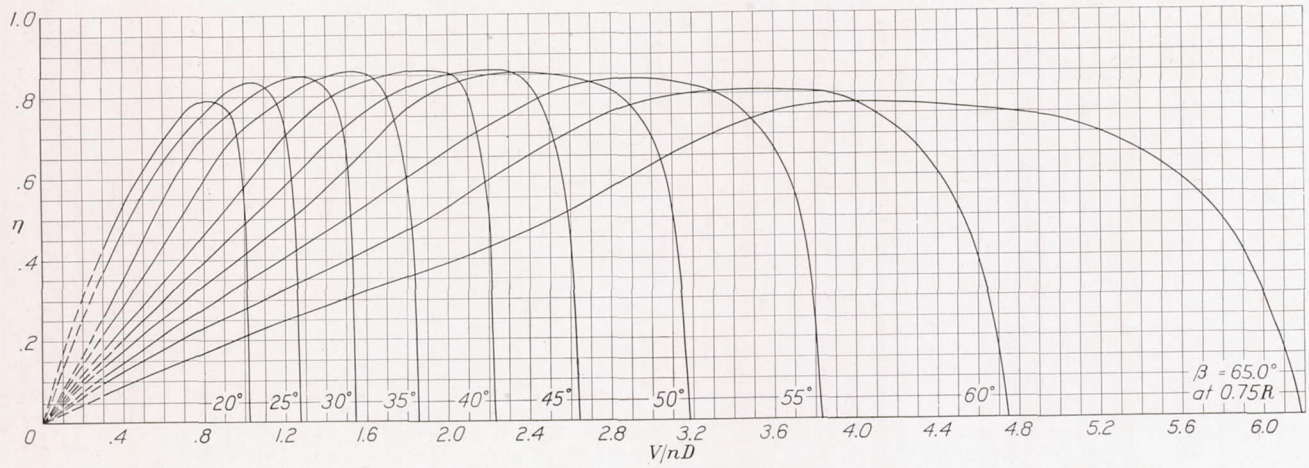
FIGURE 28.—Efficiency curves for six-blade single-rotating propeller with wing.
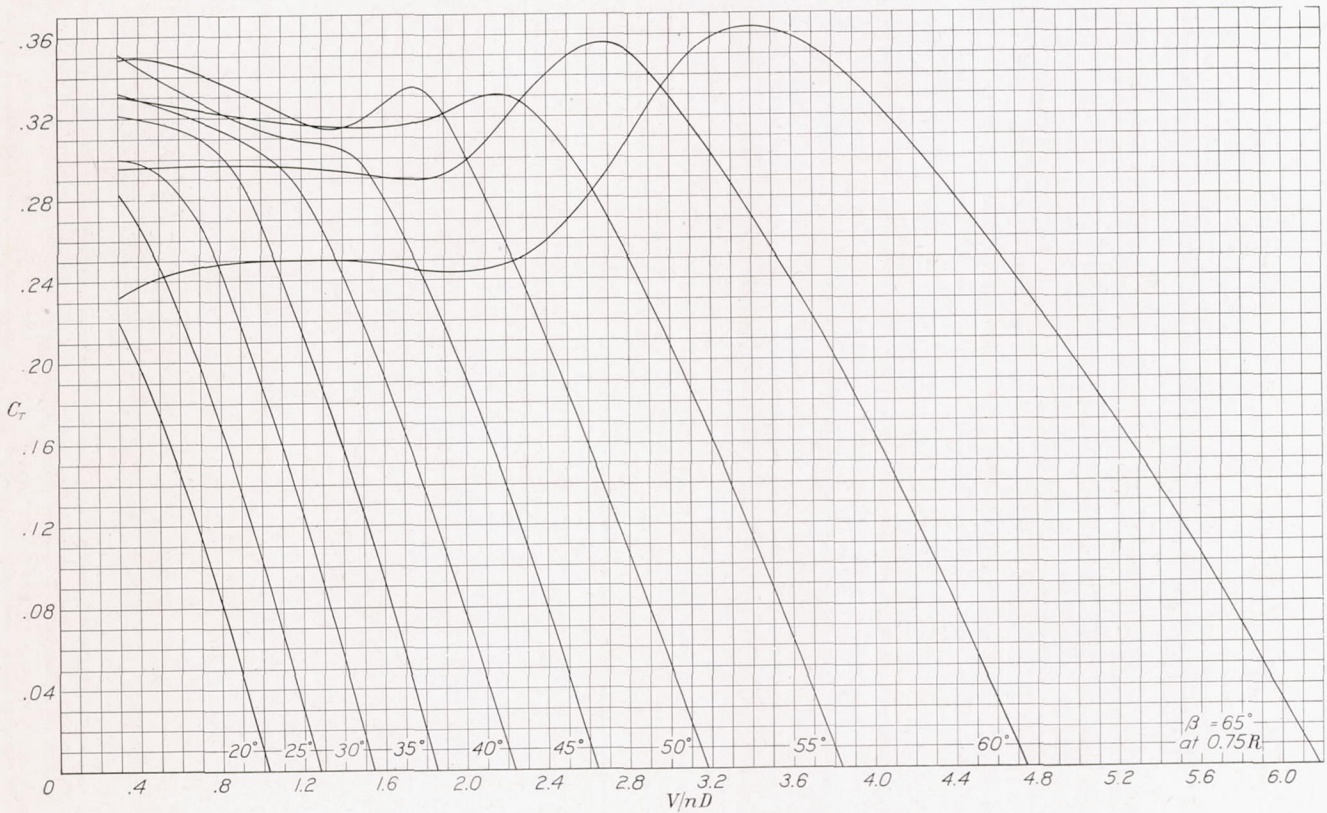
FIGURE 29.—Thrust-coefficient curves for six-blade single-rotating propeller with wing.
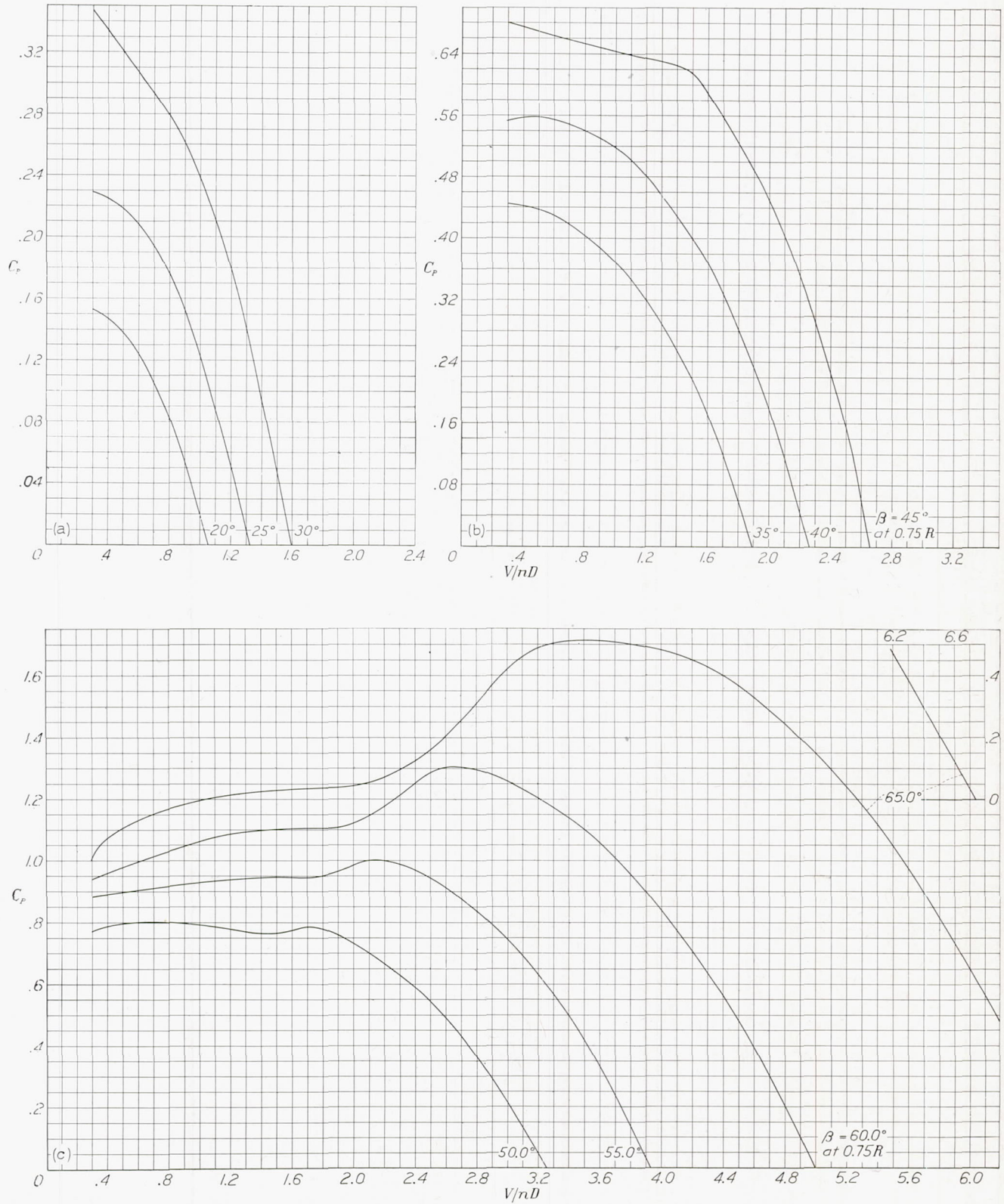
FIGURE 30.—Power-coefficient curves for six-blade single-rotating propeller with wing.
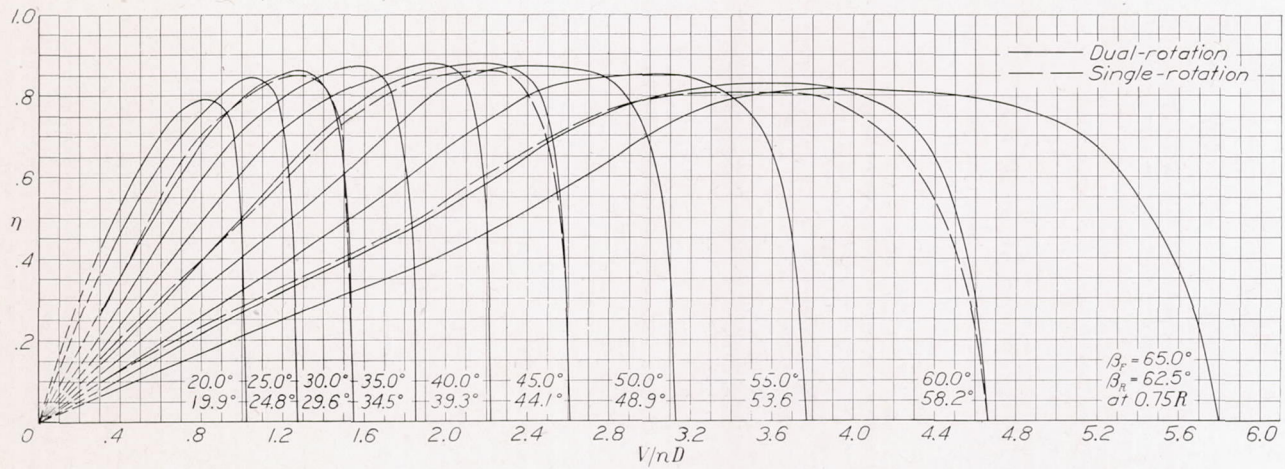
FIGURE 31.—Efficiency curves for six-blade dual-rotating propeller with wing, showing superimposed curves for the corresponding single-rotation condition at 30°, 45°, and 60° blade angles.
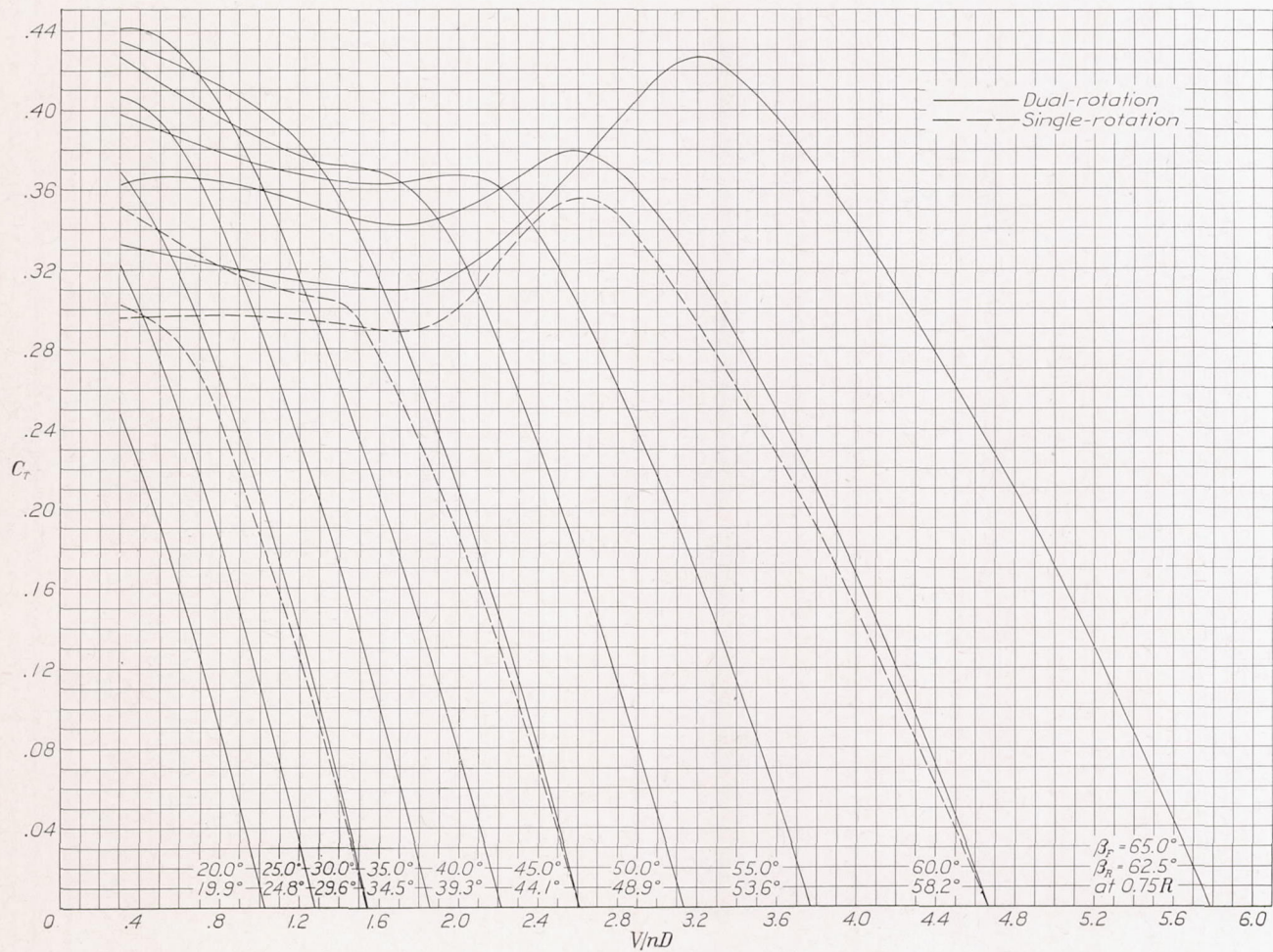
FIGURE 32.—Thrust-coefficient curves for six-blade dual-rotating propellers with wing, showing superimposed curves for the corresponding single-rotation condition at 30°, 45°, and 60° blade angles.
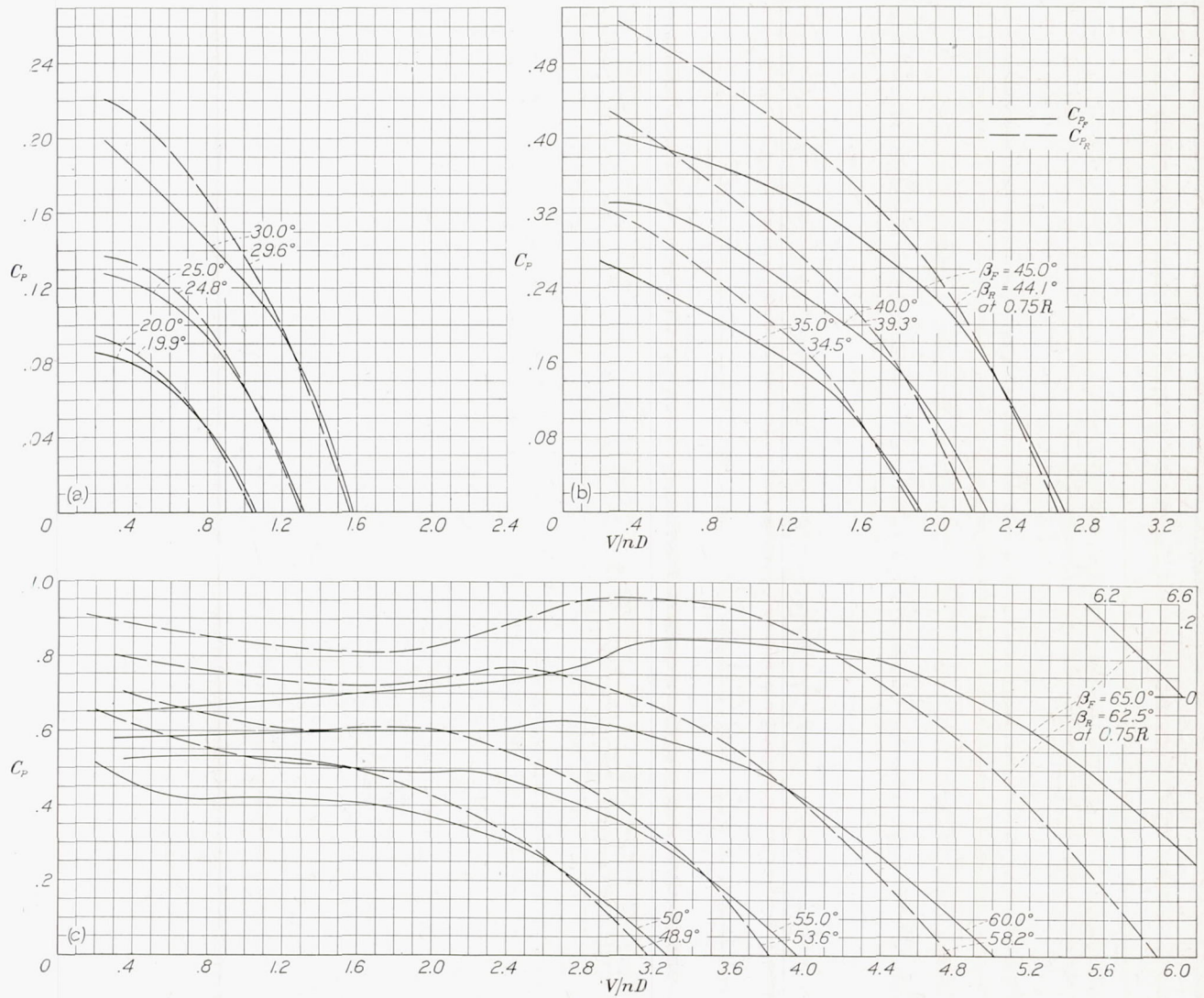
FIGURE 33.—Individual power-coefficient curves for six-blade dual-rotating propellers with wing.

(a) 30° blade angle.

(b) 45° blade angle.

(c) 60° blade angle.
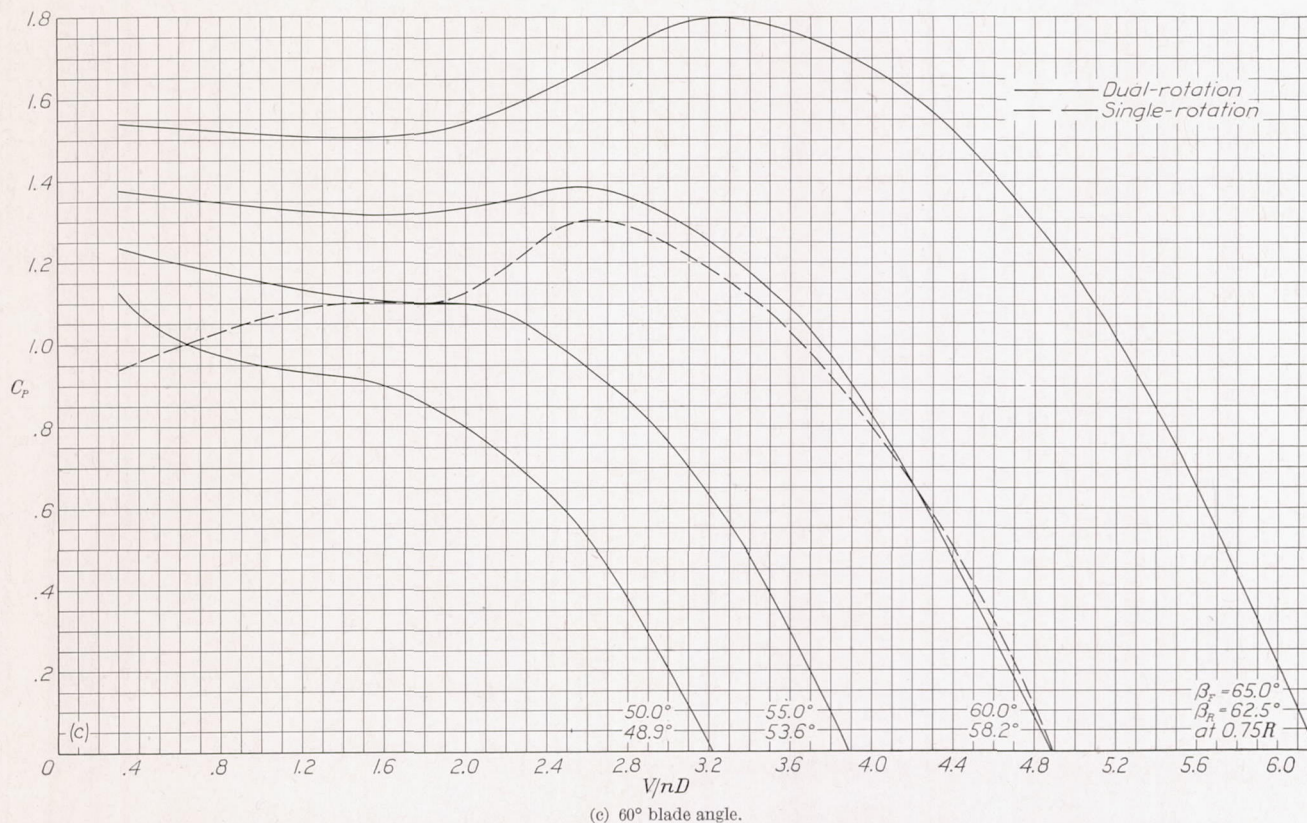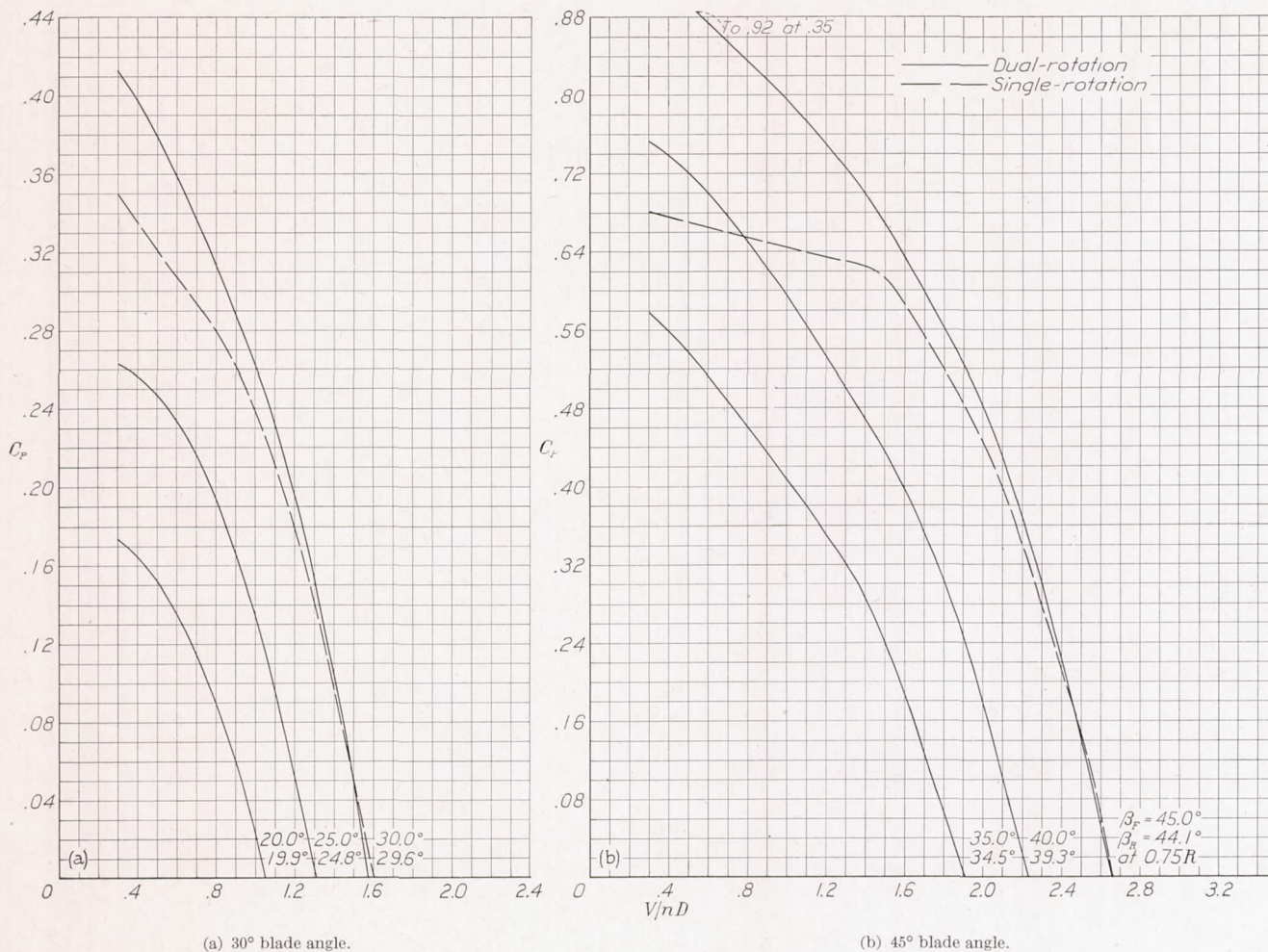
FIGURE 34.—Power-coefficient curves for six-blade dual-rotating propellers with wing, showing superimposed curve for the corresponding single-rotation condition.
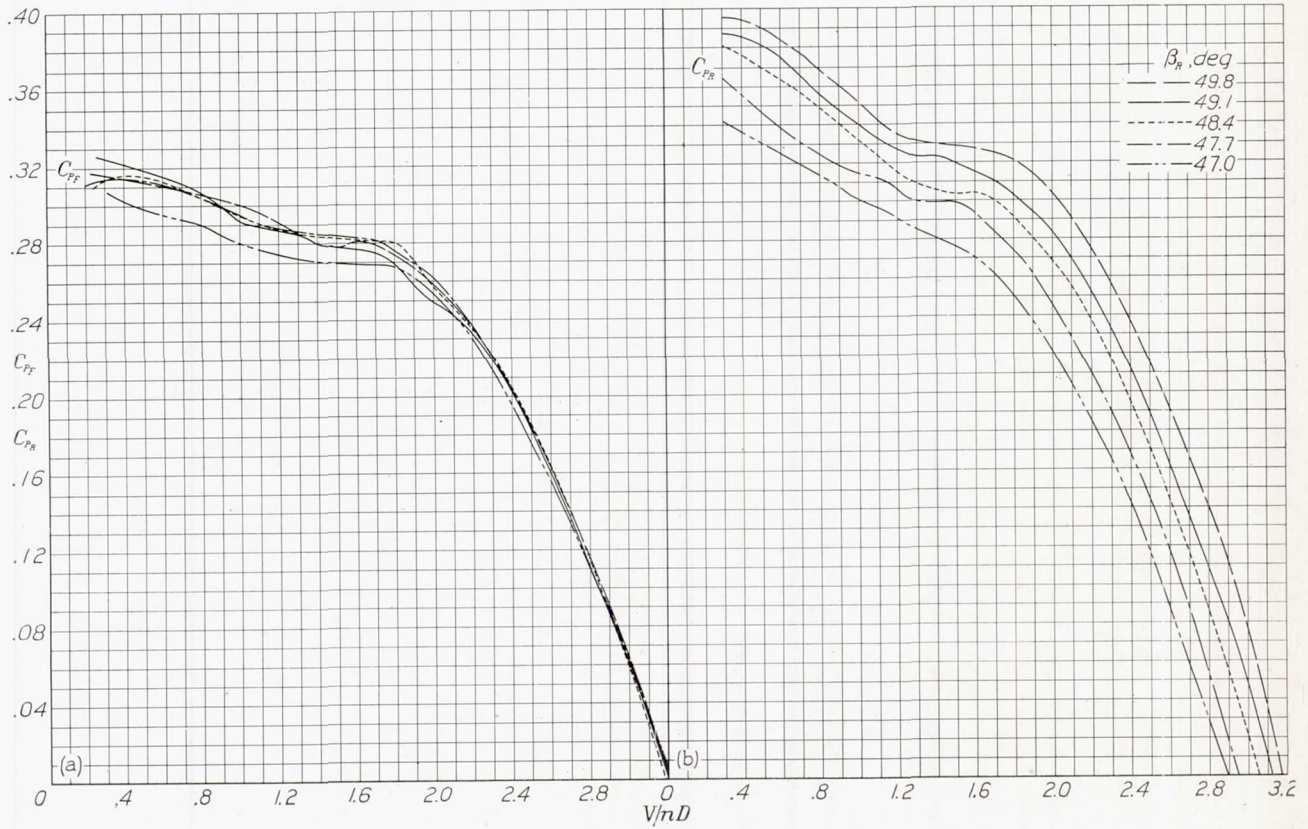
FIGURE 35.—Power-coefficient curves for the propellers showing effect of small variations in rear blade angle at a front blade angle of 50°.   (Four-blade dual-rotating propellers without wing.)
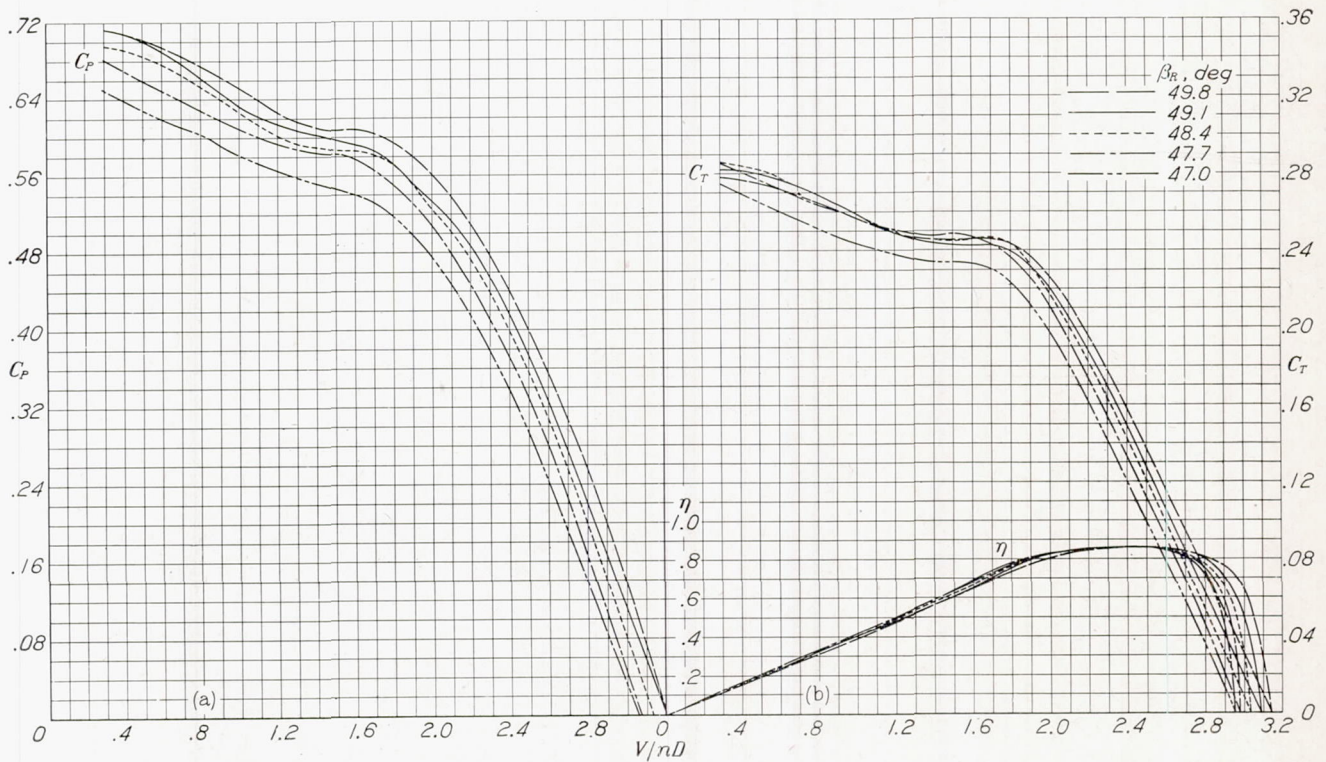
FIGURE 36.—Propeller curves showing the effect of small variations in rear blade angle at a front blade angle of 50°.   (Four-blade dual-rotating propellers without wing.)

In figures 12, 19, 26, and 33, it may be noted that the power curves for the front and the rear propellers cross at V/nD values corresponding approximately to those for peak efficiency and that at lower V/nD values the rear propeller absorbs considerably more power than the front propeller. This result further illustrates the effect of the front propeller in increasing the angle of attack of the rear propeller and indicates that the magnitude of the differences in the power absorbed by the front and the rear propellers is a direct function of the disk loading, as would be expected from theory.

In figures 35 and 36 are shown the results from a few tests made to determine the effect of small changes in the blade angle of the rear propeller. It may be noted that the thrust and the power changed, as would be expected, and that there was no measurable effect on the efficiency of the combination.

There are several important considerations in comparing single-rotating and dual-rotating propellers. The relative efficiency at all speeds is obviously of the first order of importance. The presence of a wing in the slipstream is an important consideration because it can be expected to remove about half the race rotation of a single propeller. The relative power absorbed at peak efficiency by single- and dual-rotating propellers is of some importance because of its effect on the diameter and the tip speed. The relative power absorbed at the take-off and climbing conditions determines the relative blade-angle settings and, consequently, the relative thrust. The relative thrust for a given power output is a measure of the relative efficiencies for the take-off and climb of controllable propellers.

In figure 37 are the envelope-efficiency comparisons for all conditions investigated. The four-blade dual-rotating propeller had about the same efficiency as the single-rotating propeller at a V/nD of about 1.0; but, at a V/nD of 5.0, there was a gain of 5 percent in favor of dual rotation. The wing improved the efficiency of the single-rotating propeller about 2 percent for only the high V/nD range. The wing had no effect on the four-blade dual-propeller results.

The six-blade dual-rotating propeller was from 1 to 6 percent more efficient than the single-rotating propeller. The wing improved the efficiency of the single-rotating propeller 0 to 4 percent and also improved the efficiency of the dual-rotating propeller 0 to 3 percent.

These results seem to check theory roughly in that the gain due to dual rotation, within the limits of these tests, amounts to from 0 to about 6 percent, depending upon the blade-angle setting and the disk loading. The presence of the wing resulted in about half as much improvement in efficiency as dual rotation.

In figure 37 is also shown the effect of different numbers of blades on efficiency. The results for the two- and three-blade propellers, which are included here for comparison, are the average of the results of the tests made with the propellers located in the front and the rear positions. Inasmuch as the rear spinner is larger than the front one, the efficiency of the rear propeller was found to be 1 or 2 percent higher than that of the front one. The use of average results for the two- and three-blade propellers makes possible a direct comparison with the four- and six-blade propellers, each of which was made up with half the blades located in the front and half in the rear position.
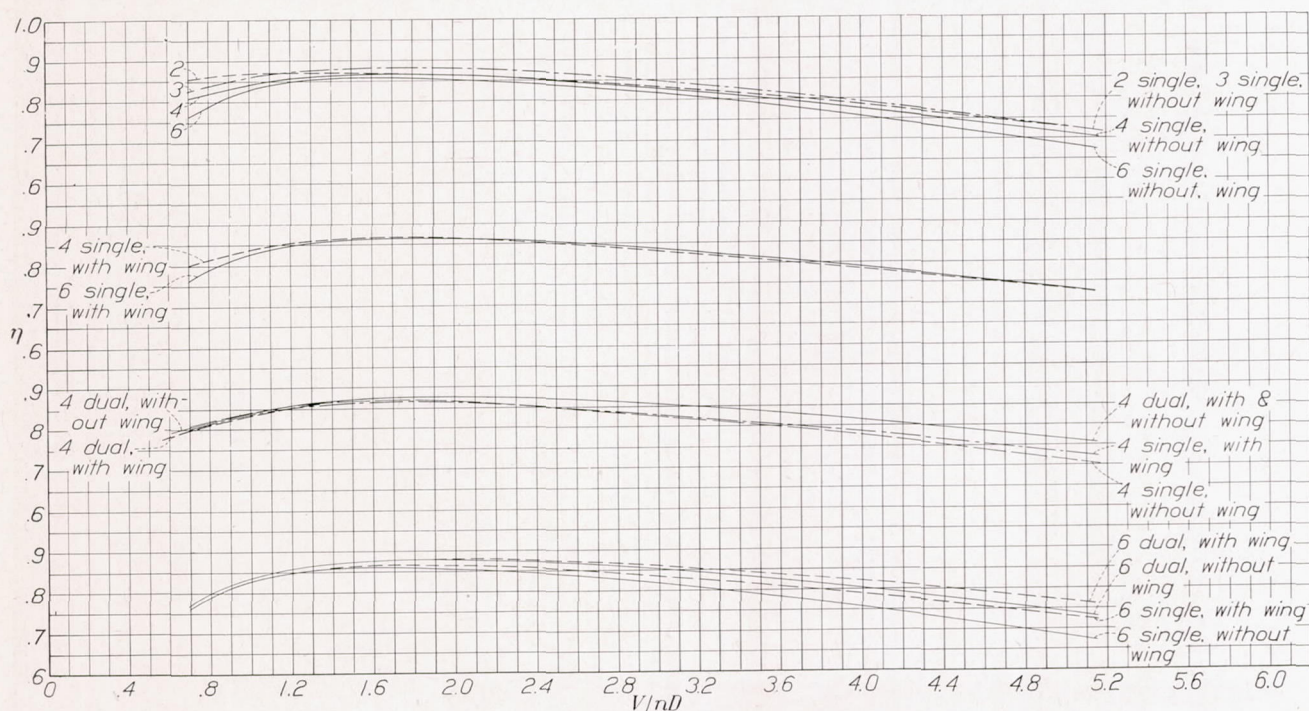
FIGURE 37.—Comparison of efficiency-envelope curves for the propellers tested.
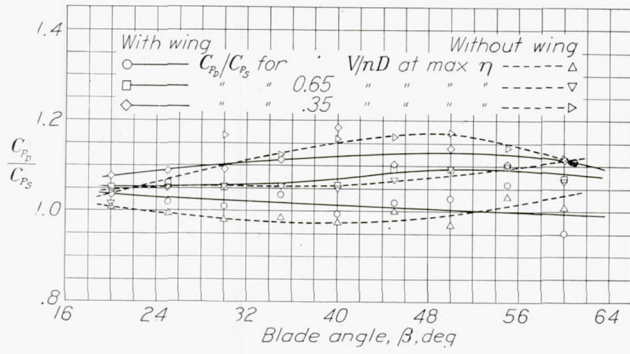
FIGURE 38.—Ratio of $\dfrac{C_P \text{ for dual rotation}}{C_P \text{ for single rotation}}$ in take-off, climb, and at peak efficiency for the four-blade propeller.
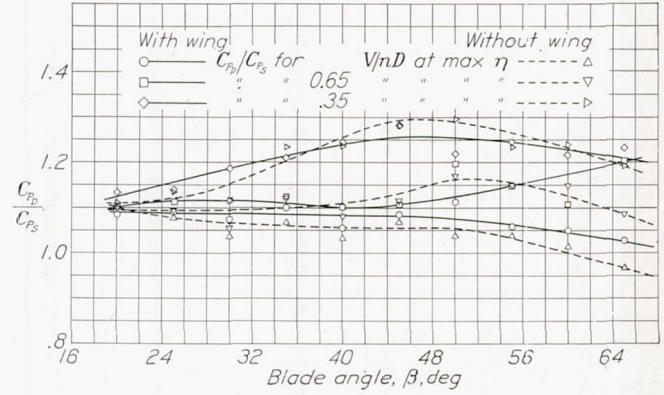
FIGURE 39.—Ratio of $\dfrac{C_P \text{ for dual rotation}}{C_P \text{ for single rotation}}$ in take-off, climb, and at peak efficiency for the six-blade propeller.
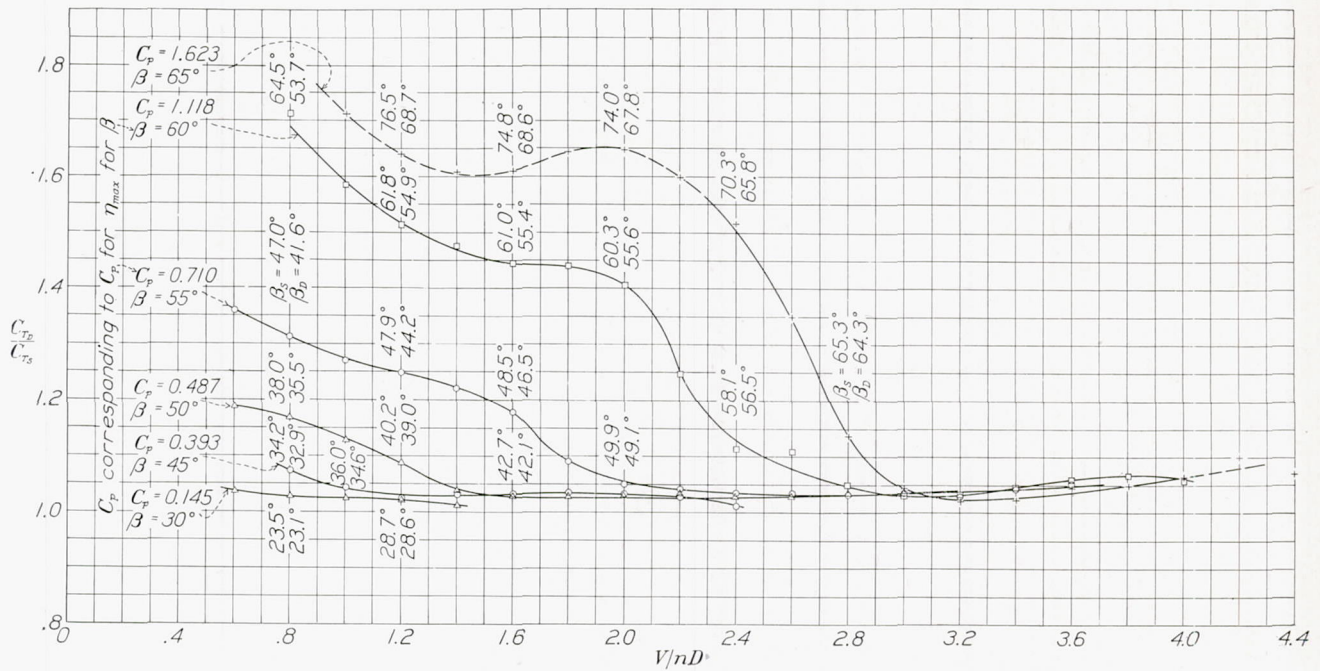
FIGURE 40.—Ratio of $\dfrac{C_T \text{ for dual rotation}}{C_T \text{ for single rotation}}$ for constant values of C_P.   Six-blade propellers without wing.
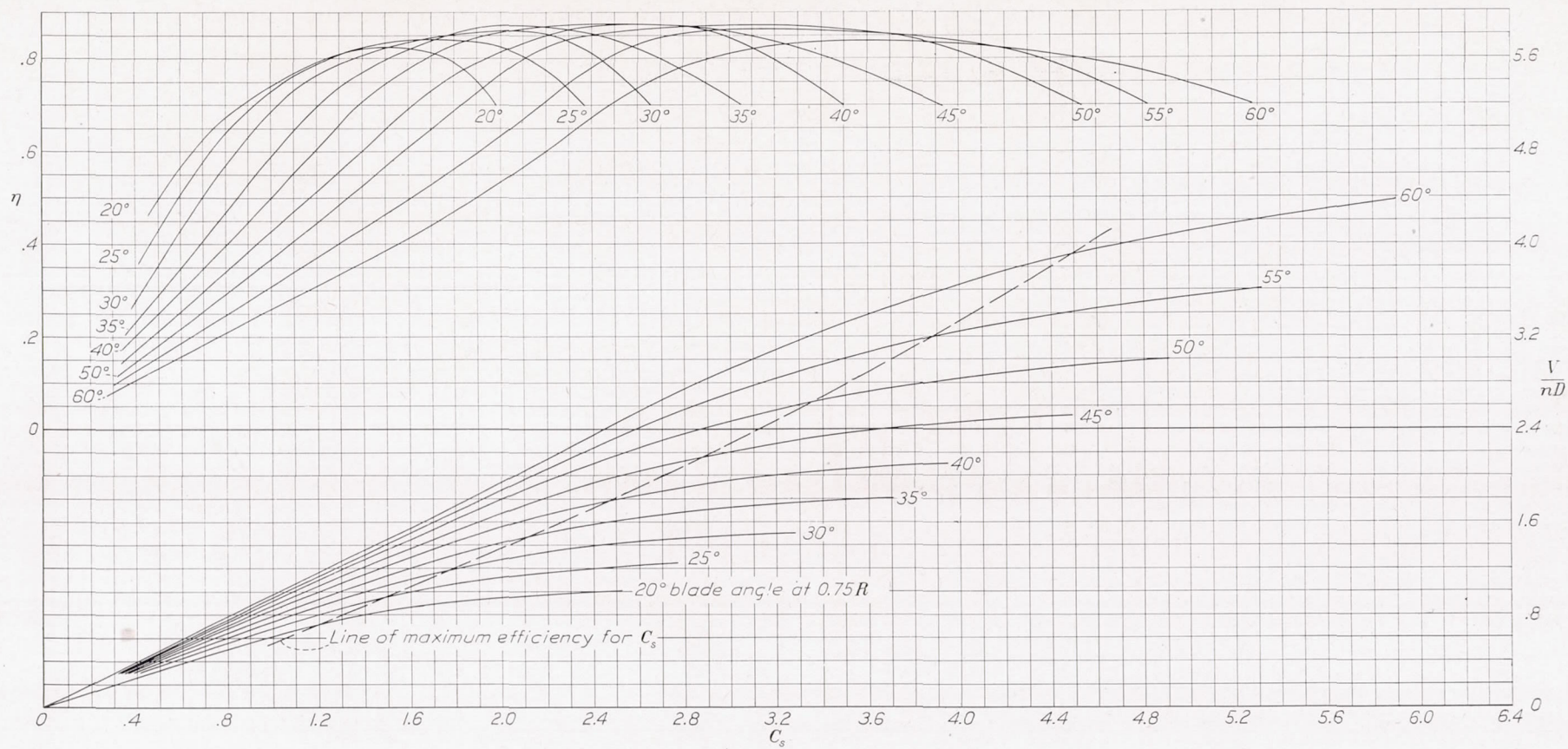
FIGURE 41.—Design chart for propellers 3155–6 and 3156–6, four-blade dual rotation without wing.
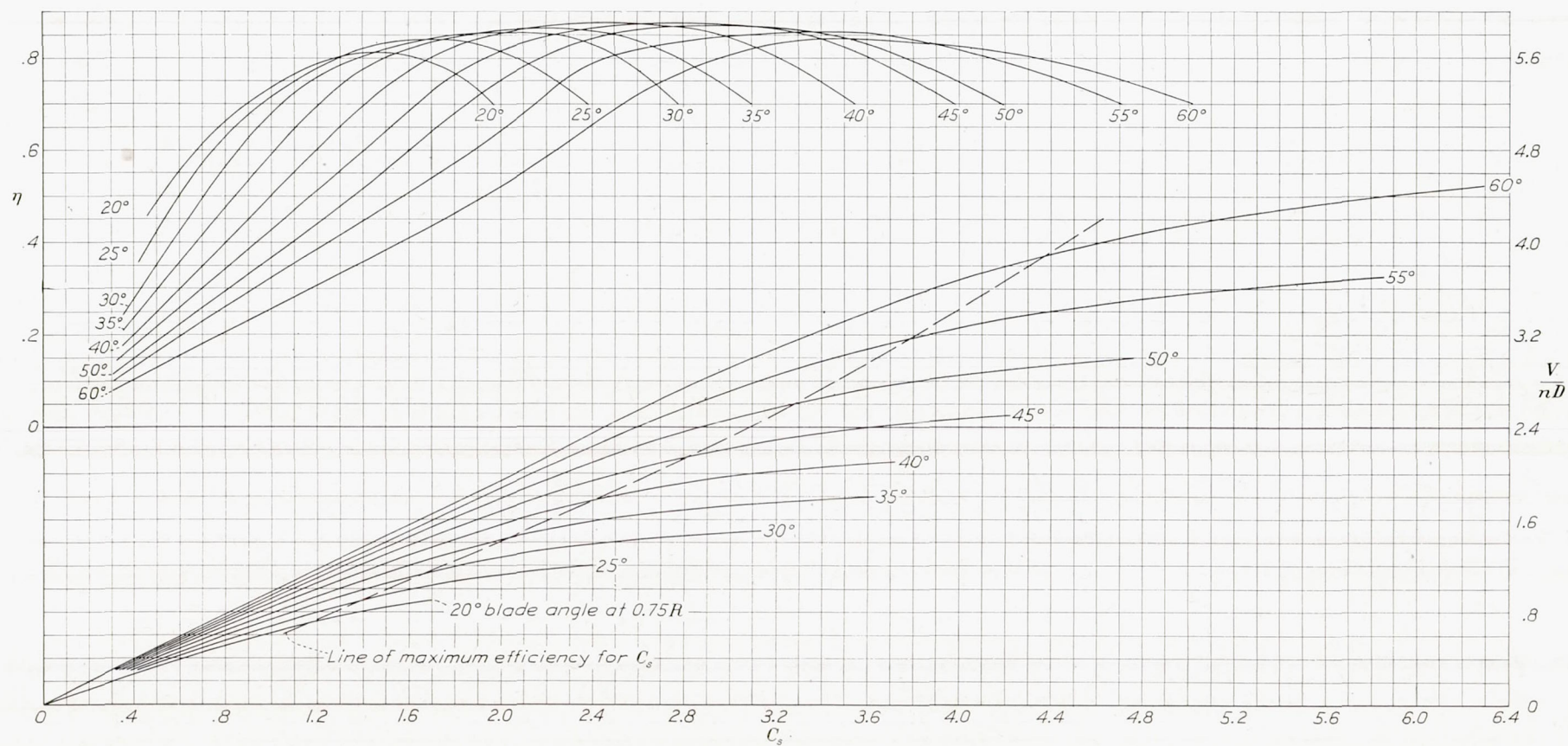
FIGURE 42.—Design chart for propellers 3155–6 and 3156–6, four-blade dual rotation with wing.
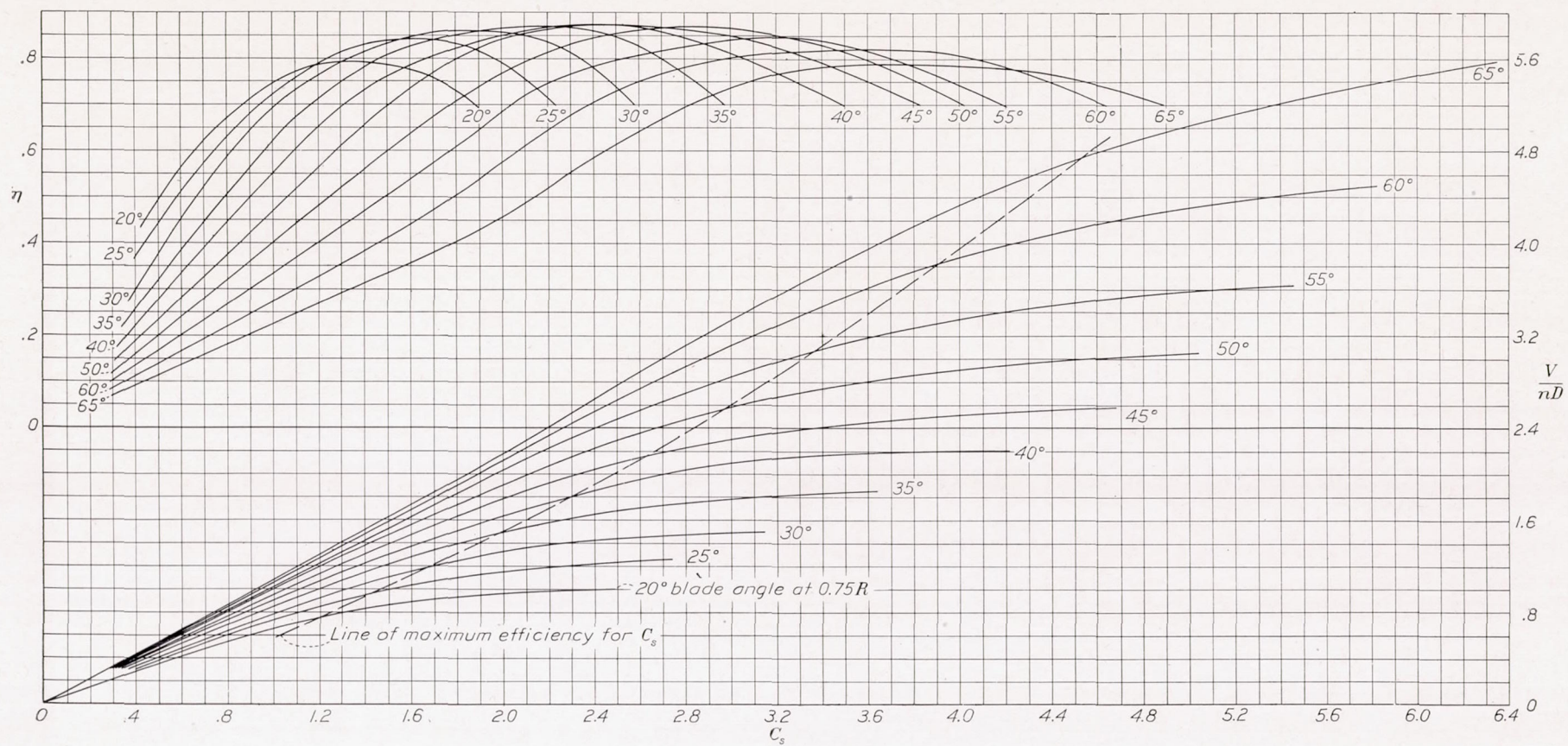
FIGURE 43.—Design chart for propellers 3155–6 and 3156–6, six-blade dual rotation without wing.
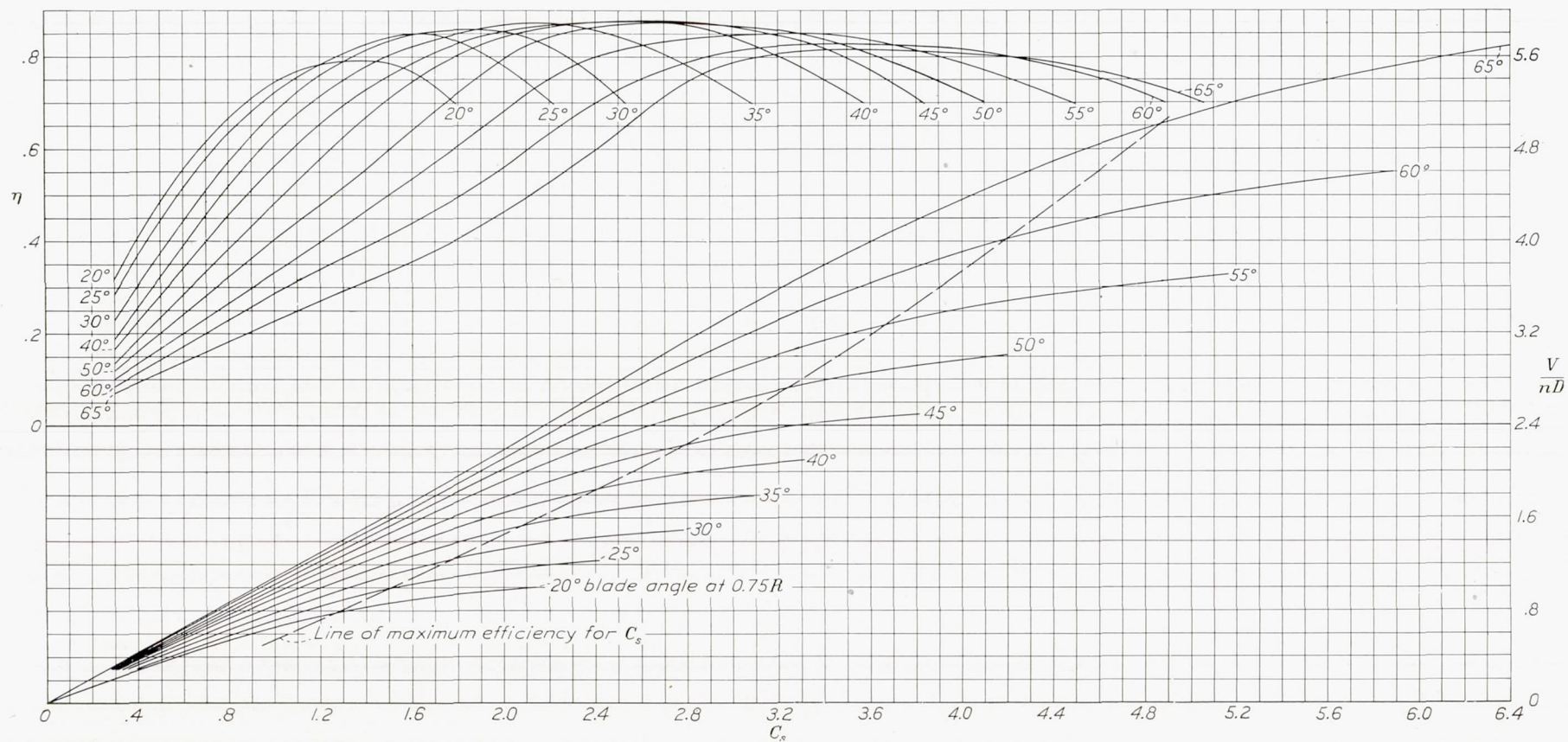
FIGURE 44.—Design chart for propellers 3155–6 and 3156–6, six-blade dual rotation with wing.

There was very little difference between the efficiencies of the two-, three-, four-, and six-blade propellers except for the low V/nD range. At high values of V/nD the six-blade propeller was only about 2 percent less efficient than the three-blade one. It should be pointed out, however, that solidity comparisons of this type do not necessarily bring out the true significance, inasmuch as the disk loading was not the same for each propeller.

The relative power absorbed by single-rotating and dual-rotating propellers is given in figures 38 and 39 for three flight conditions. The comparisons are made on the basis of the same effective blade angles; namely, the dual-propeller results were interpolated to bring the V/nD for zero thrust in coincidence with that for the single propeller. The results indicate that the four-blade single and dual propellers absorbed about the same power for the peak-efficiency condition; but that at V/nD values corresponding to the take-off and climbing conditions the dual-rotating propeller absorbed 5 to 17 percent more power than the single-rotating propeller. The six-blade comparison (fig. 39) shows more pronounced effects, even for the high-speed condition; the dual propeller absorbed several percent more power for the high-speed condition and as much as 30 percent more power for the take-off condition. This result indicates either that the diameter of the dual propeller will be smaller than that of the single one for equal power absorption or that the blade angles for the take-off and climbing conditions will be lower.

The relative thrust available for dual-rotating and single-rotating propellers operating at equal values of C_P is given in figure 40. These curves show a true comparison of controllable propellers of equal diameter operating at all flight speeds but at constant torque, engine speed, and altitude and, consequently, show the direct effect of dual-rotating propellers on the thrust for the take-off and climbing conditions. Relative thrust curves are given for several airplane categories, defined by the blade-angle settings for high speed. Thus blade angles of 30°, 45°, 50°, 55°, 60°, and 65° correspond roughly to speeds of 250, 375, 425, 450, 500, and 525 miles per hour, respectively, if a tip speed of 900 to 1000 feet per second is assumed. Inasmuch as the engine speed and diameter are assumed constant, the V/nD is directly proportional to the airspeed.

This analysis indicates that there is a marked gain due to dual rotation for the take-off and climb of airplanes operating at conditions of C_P greater than 0.4 or for conditions wherein the blade angles for take-off and climb exceed 30°. In terms of airplane categories, the take-off and climbing thrust of airplanes having high speeds at sea level in excess of about 375 miles per hour would be benefited by dual-rotating propellers. Airplanes having high speeds at 20,000 feet greater than about 460 miles per hour would have take-off blade angles (assuming equal power) in excess of 30° and

consequently would benefit by dual rotation for this condition; the benefit would be even greater for the climbing condition at 20,000 feet.

A sample calculation will illustrate this point. Given: High speed of 500 miles per hour at 20,000 feet

β for high speed $= 60°$
V/nD for high speed $= 3.6$
C_P for high speed $= 1.118$

To find relative thrust at reduced speeds:

V/nD for climb at 20,000 feet $= 3.6 \times 0.65 = 2.34$
$C_{T_D}/C_{T_S} = 1.2$ (climb at 20,000 ft)
C_P for sea level $= 0.595$ (assuming constant engine power)
$C_{T_D}/C_{T_S} = 1.06$ (climb at sea level)
V/nD for take-off $= 0.35 \times 3.6 = 1.26$ (assuming constant engine speed)
$C_{T_D}/C_{T_S} = 1.15$

CONCLUSIONS

These conclusions apply to the present test conditions wherein the blades of the front and rear propellers were set to absorb equal power only at peak efficiency.

1. The peak efficiency of dual-rotating four- and six-blade tractor propellers was found to be from 0 to 6 percent greater than that of single-rotating propellers, depending upon the disk loading and the blade-angle setting; the higher these values, the greater the difference in efficiency up to the limiting test blade angle of 65°.

2. The maximum efficiency of a single-rotating propeller was increased by installing a wing in the slipstream. Dual rotation (without wing) yielded a gain of approximately twice as much.

3. Dual-rotating propellers absorbed only slightly more power at peak efficiency than did single-rotating ones; but at Vn/D values corresponding to the take-off and climbing conditions the difference was more pronounced.

4. The take-off and climbing thrusts of dual-rotating controllable propellers for airplanes in the category of 400 miles per hour and up were found to exceed the values for single-rotating propellers by substantial margins.

REFERENCES

1. Weinig, Fritz: Gegenläufige Schrauben für Flugzeuge. Jahrb. 1937 der deutschen Luftfahrtforschung, R. Oldenbourg (Munich), pp. I 215–I 223.
2. Lazzarino, Lucio: Study of Airscrews for High Speed Aeroplanes. R. A. S. Jour., vol. XLIV, no. 352, April 1940, pp. 322-327.
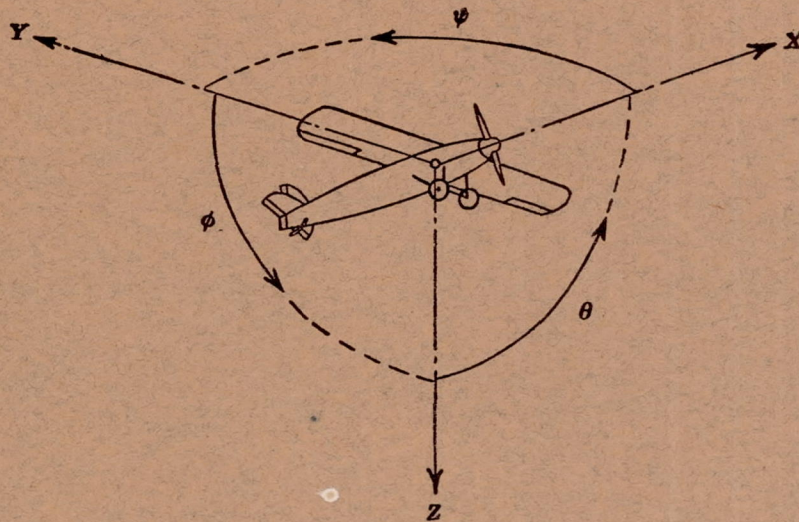
Positive directions of axes and angles (forces and moments) are shown by arrows

Axis		Force (parallel to axis) symbol	Moment about axis			Angle		Velocities	
Designation	Symbol		Designation	Symbol	Positive direction	Designation	Symbol	Linear (component along axis)	Angular
Longitudinal	X	X	Rolling	L	$Y \longrightarrow Z$	Roll	φ	u	p
Lateral	Y	Y	Pitching	M	$Z \longrightarrow X$	Pitch	θ	v	q
Normal	Z	Z	Yawing	N	$X \longrightarrow Y$	Yaw	ψ	w	r

Absolute coefficients of moment

$$C_l = \frac{L}{qbS} \qquad C_m = \frac{M}{qcS} \qquad C_n = \frac{N}{qbS}$$
$$\text{(rolling)} \qquad \text{(pitching)} \qquad \text{(yawing)}$$

Angle of set of control surface (relative to neutral position), δ. (Indicate surface by proper subscript.)

4. PROPELLER SYMBOLS

D Diameter
p Geometric pitch
p/D Pitch ratio
V' Inflow velocity
V_s Slipstream velocity

T Thrust, absolute coefficient $C_T = \dfrac{T}{\rho n^2 D^4}$

Q Torque, absolute coefficient $C_Q = \dfrac{Q}{\rho n^2 D^5}$

P Power, absolute coefficient $C_P = \dfrac{P}{\rho n^3 D^5}$

C_s Speed-power coefficient $= \sqrt[5]{\dfrac{\rho V^5}{P n^2}}$

η Efficiency
n Revolutions per second, rps

Φ Effective helix angle $= \tan^{-1}\left(\dfrac{V}{2\pi rn}\right)$

5. NUMERICAL RELATIONS

1 hp = 76.04 kg-m/s = 550 ft-lb/sec
1 metric horsepower = 0.9863 hp
1 mph = 0.4470 mps
1 mps = 2.2369 mph

1 lb = 0.4536 kg
1 kg = 2.2046 lb
1 mi = 1,609.35 m = 5,280 ft
1 m = 3.2808 ft